Monthly Notices
of the
ROYAL ASTRONOMICAL SOCIETY

MNRAS **441,** 886–899 (2014) doi:10.1093/mnras/stu585

The extent of the Mg II absorbing circumgalactic medium of quasars★

E. P. Farina,[1,2,3]† R. Falomo,[4] R. Scarpa,[5] R. Decarli,[3] A. Treves[1,2]‡ and J. K. Kotilainen[6]

[1]*Università degli Studi dell'Insubria – via Valleggio 11, I-22100 Como, Italy*
[2]*INFN Milano–Bicocca – Università degli Studi di Milano–Bicocca, Piazza della Scienza 3, I-20126 Milano, Italy*
[3]*Max–Planck–Institut für Astronomie – Königstuhl 17, D-69117 Heidelberg, Germany*
[4]*INAF – Osservatorio Astronomico di Padova, Vicolo dell'Osservatorio 5, I-35122 Padova, Italy*
[5]*Instituto de astrofisica de Canarias – c/via Lactea s/n, E-38205 San Cristobal de la Laguna, Spain*
[6]*Finnish Centre for Astronomy with ESO (FINCA) – University of Turku, Väisäläntie 20, FI-21500 Piikkiö, Finland*

Accepted 2014 March 24. Received 2014 March 24; in original form 2013 May 14

ABSTRACT

We investigate the extent and the properties of the Mg II cool, low-density absorbing gas located in the halo and in the circumgalactic environment of quasars, using a sample of 31 projected quasar pairs with impact parameter pd < 200 kpc in the redshift range $0.5 \lesssim z \lesssim 1.6$. In the transverse direction, we detect 18 Mg II absorbers associated with the foreground quasars, while no absorption system originated by the gas surrounding the quasar itself is found along the line of sight. This suggests that the quasar emission induces an anisotropy in the absorbing gas distribution. Our observations indicate that the covering fraction (f_C) of Mg II absorption systems with rest-frame equivalent width $W_r(\lambda 2796) > 0.3$ Å ranges from $f_C \sim 1.0$ at pd $\lesssim$ 65 kpc to $f_C \sim 0.2$ at pd $\gtrsim 150$ kpc, and appears to be higher than that for galaxies. Our findings support a scenario where the luminosity/mass of the host galaxies affect the extent and the richness of the absorbing Mg II circumgalactic medium.

Key words: galaxies: haloes – quasars: absorption lines – quasars: general.

1 INTRODUCTION

Major mergers between galaxies are believed to be responsible for intense starbursts in galaxies and for channelling large amount of gas down to the circumnuclear regions that trigger the activity of the central supermassive black hole (SMBH; e.g.Hernquist 1989; Kauffmann & Haehnelt 2000; Canalizo & Stockton 2001; Di Matteo, Springel & Hernquist 2005; Hennawi et al. 2006a; Bennert et al. 2008). In this scenario, the circumgalactic medium (CGM) of quasars is expected to harbour a large amount of enriched gas (e.g. Prochaska, Hennawi & Simcoe 2013a) and its study offers an opportunity to investigate the link between the nuclear activity of quasars and their immediate environment.

The study of absorption lines represents a powerful way to probe the quasar CGM (e.g. Shaver, Boksenberg & Robertson 1982; Shaver & Robertson 1983, 1985; Bowen et al. 2006; Hennawi et al. 2006b; Hennawi & Prochaska 2007; Decarli, Treves & Falomo 2009; Prochaska & Hennawi 2009; Tytler et al. 2009; Farina et al. 2013), since it is typically too dim to be detected directly (Chelouche et al. 2008; Hennawi & Prochaska 2013). In particular, the Mg II λλ2796, 2803 doublet is well suited for this aim. It falls within the optical wavelength range at intermediate redshift, probes regions of metal enriched, photoionized gas at temperatures around T $\sim 10^4$ K (Bergeron & Stasińska 1986; Charlton et al. 2003), and traces a wide range of neutral hydrogen column densities (i.e. from $N_{\rm H\,I} \sim 10^{16.5}$ cm^{-2} to greater than $N_{\rm H\,I} \sim 10^{21.5}$ cm^{-2}; e.g. Bergeron & Stasińska 1986; Rao & Turnshek 2000; Rao, Turnshek & Nestor 2006).

Observations of low-redshift galaxies ($z \lesssim 1$) showed the presence of a large halo of cool Mg II absorbing gas, extending up to ∼200 kpc (e.g. Bahcall & Spitzer 1969; Boksenberg & Sargent 1978; Steidel, Dickinson & Persson 1994; Steidel et al. 1997; Churchill, Kacprzak & Steidel 2005; Chen et al. 2010a,b; Bowen & Chelouche 2011; Nielsen, Churchill & Kacprzak 2013b; Nielsen et al. 2013a), which is strongly linked to galaxy properties such as: luminosity (e.g. Chen & Tinker 2008; Chen et al. 2010a); mass (e.g. Bouché et al. 2006; Chen et al. 2010b; Churchill et al. 2013a); colour (e.g. Zibetti et al. 2007); star formation rate (e.g. Prochter, Prochaska & Burles 2006; Ménard et al. 2011; Nestor et al. 2011); morphology (e.g. Kacprzak et al. 2007); and galactic environment (e.g. Bordoloi et al. 2011). These findings have motivated the search for possible mechanism responsible for the enrichment of the CGM at such large scale. Detailed studies of the kinematics of

★Based on observations made with the Gran Telescopio Canarias (GTC), installed in the Spanish Observatorio del Roque de los Muchachos of the Instituto de Astrofísica de Canarias, in the island of La Palma.
† E-mail: emanuele.paolo.farina@gmail.com
‡ Associated to INAF.

the absorption systems have shown that both outflows due to galactic wind (e.g. Tremonti, Moustakas & Diamond-Stanic 2007; Weiner et al. 2009; Rubin et al. 2010) and inflows on to the galaxies (e.g. Ribaudo et al. 2011; Rubin et al. 2012) could supply the CGM of cool enriched gas.

In this paper, we extend these studies to quasar host galaxies: if two quasars are angularly close but have discordant redshifts, one can probe the CGM of the foreground target (QSO_F) through the study of absorption features imprinted on spectra of the background source (QSO_B). This technique has allowed a detailed study of the distribution of neutral hydrogen around quasars. For instance, Hennawi et al. (2006b), starting from a sample of 149 projected quasar pairs (projected distance: 30 kpc $\lesssim$ pd $\lesssim$ 2.5 Mpc; redshift: $1.8 < z < 4.0$), found that the probability to have an absorber with $N_{\rm H\,I} > 10^{19}$ cm^{-2} coincident within 200 kpc with a QSO_F is high (∼50 per cent), and that the distribution of these absorbers is highly anisotropic (Hennawi & Prochaska 2007). Considering a larger sample of pairs Prochaska et al. (2013a) and Prochaska et al. (2013b) recently confirm the presence of a large number of absorbers with $N_{\rm H\,I} > 10^{17.3}$ cm^{-2} in the proximity of quasars.

It is worth noting that the quasar host galaxies are typically more massive than normal galaxies and may trace group/cluster environments (e.g. Wold et al. 2001; Serber et al. 2006; Hutchings, Scholz & Bianchi 2009); hence, their CGM is expected to be richer and could exhibit different physical characteristics. In addition, the presence of the central SMBH may have a substantial effect. In fact its emission may photoionize gas from tens to several hundreds of kpc and photoevaporate cool clumps (e.g. Hennawi & Prochaska 2007; Chelouche et al. 2008; Wild et al. 2008; Farina et al. 2013).

The first attempt to explore the Mg II absorbing CGM of quasars was performed by Bowen et al. (2006), who detected absorption lines in all the four close projected quasar pairs investigated. In Farina et al. (2013), we have studied 10 additional systems, exploring projected separations between 60 and 120 kpc. Here, we aim to further expand this work and to extend it up to separations of 200 kpc, in order to determine the gas covering fraction and the size of the haloes hosting quasars. The new sample of projected quasar pairs is described in Section 2 and the analysis of the collected spectra in Section 3. In Section 4, we investigate the properties of the detected Mg II absorption systems. We compare and contrast our results with those found in inactive galaxies in Section 5 and we summarize our conclusions in Section 6.

Throughout this paper, we assume a concordance cosmology with $H_0 = 70\,{\rm km\,s^{-1}Mpc^{-1}}$, $\Omega_{\rm m} = 0.3$, and $\Omega_\Lambda = 0.7$.

2 THE SAMPLE

In order to study the CGM of quasars in absorption, we searched in the Schneider et al. (2010) catalogue (based on the 7th data release of the Sloan Digital Sky Survey, SDSS; Abazajian et al. 2009) for quasar pairs that have physical projected separations pd < 200 kpc (calculated in the frame of the foreground targets) and line-of-sight (LOS) velocity differences $\Delta V > 5000\,{\rm km\,s^{-1}}$. 17 of the 85 retrieved systems were observed with the intermediate-resolution grisms R2500V and R2500R of the Optical System for Imaging and low Resolution Integrated Spectroscopy (OSIRIS; Cepa et al. 2000, 2003) mounted on the 10.4 m Gran Telescopio de Canarias (GTC). We have selected these targets to have the Mg II doublet lines at $z = z_F$ well within the spectral range covered by the two considered grisms (nominally from 4470 to 5950 Å for R2500V and from 5630 to 7540 Å for R2500R). This constrains the QSO_F redshifts in the range $0.6 \lesssim z_F \lesssim 1.6$. Data for an additional pair (QQ01, see Table 1) were collected with the grism 1400V of the FOcal Reducer and low dispersion Spectrograph (FORS2;

Table 1. Properties of the observed projected quasar pairs: our identification label of the system (ID), position of the foreground target (RA, DEC.), redshift derived from broad emission lines (z), SDSS BEST AB r-band magnitude (r; Abazajian et al. 2009), angular ($\Delta\theta$) and projected (pd) separation between the two quasars, bolometric luminosity ($L_{\rm bol}$, see Appendix A for details), black hole mass ($M_{\rm BH}$; see Vestergaard & Peterson 2006 and Appendix A for details) and host galaxy mass ($M_{\rm host}$ derived from $M_{\rm BH}$; see Decarli et al. 2010b and text for details) of the foreground quasar, seeing during the observations (See.), and signal-to-noise ratio per pixel on the continuum close to the expected position of the Mg II absorption lines (S/N). The labels F and B refer to the foreground and background quasar, respectively.

ID	RA_F (J2000)	$DEC._F$ (J2000)	z_F	z_B	r_F (mag)	r_B (mag)	$\Delta\theta$ (arcsec)	pd (kpc)	$L_{\rm bol,F}$ (10^{46} erg s^{-1})	$M_{\rm BH,F}$ (10^8 M$_\odot$)	$M_{\rm host,F}$ (10^{11} M$_\odot$)	See. (arcsec)	S/N_F	S/N_B
QQ01[a]	00:38:23.8	−29:13:11	0.793	2.699	19.54[b]	19.87[b]	12.1	91	0.09±0.01	1.9	0.9	1.2	11	11
QQ02	00:47:57.2	+14:47:42	1.620	2.746	19.17	19.07	9.4	80	1.95±0.14	3.3	0.9	1.0	15	12
QQ03	00:49:51.9	+00:03:44	1.121	1.332	19.13	19.71	21.4	175	1.04±0.08	7.5	2.9	0.9	32	22
QQ04	01:03:48.1	+15:01:57	1.319	1.744	18.89	17.47	22.2	186	2.14±0.09	17.1	5.9	1.1	33	43
QQ05	01:35:00.8	−00:40:54	1.003	1.259	19.55	19.10	22.0	176	0.23±0.04	2.9	1.2	1.4	10	9
QQ06	01:46:30.1	+00:15:21	0.923	1.019	20.12	18.67	15.9	125	0.30±0.06	3.3	1.5	0.8	11	17
QQ07	02:15:52.5	+01:10:00	0.875	2.215	19.60	20.01	18.8	145	0.35±0.03	1.3	0.6	0.8	22	13
QQ08	02:19:53.0	−00:44:34	0.685	1.035	19.22	19.22	19.5	138	0.18±0.02	2.4	1.3	0.8	14	10
QQ09	02:21:58.7	−00:10:44	1.036	3.213	19.87	20.03	8.2	66	0.31±0.03	4.1	1.7	0.9	18	17
QQ10	02:29:47.1	−00:53:32	0.727	2.307	20.55	20.09	16.0	116	0.10±0.01	0.8	0.4	0.9	11	8
QQ11	02:46:03.6	−00:32:11	1.600	2.161	18.47	20.13	22.0	176	2.14±0.07	10.1	2.9	1.1	22	6
QQ12	03:38:54.2	−00:23:17	1.189	2.664	20.16	19.99	17.8	147	0.25±0.03	6.3	2.4	1.4	12	10
QQ13	16:24:49.6	+49:30:32	0.634	2.275	19.33	19.74	28.6	196	0.14±0.01	6.1	3.3	0.8	25	17
QQ14	16:26:07.1	+14:00:27	1.103	2.341	19.50	19.59	19.0	156	0.58±0.02	1.7	0.7	0.8	18	22
QQ15	16:41:45.2	+27:36:22	0.920	1.649	19.18	18.61	21.7	170	0.51±0.04	1.5	0.7	0.9	15	20
QQ16	22:06:44.4	−00:39:06	1.228	1.514	19.54	19.72	13.1	109	0.71±0.03	7.1	2.6	0.8	28	19
QQ17	22:59:02.9	+00:32:44	0.868	1.465	20.04	19.66	23.7	183	0.26±0.03	3.8	1.8	0.8	13	9
QQ18	23:53:15.0	−00:50:34	1.427	1.946	19.14	19.50	23.6	199	0.79±0.07	5.4	1.8	0.9	34	32

[a] Quasar pair observed with FORS2 at ESO-VLT.
[b] R-band magnitude from the USNO-B catalogue, first epoch (Monet et al. 2003).

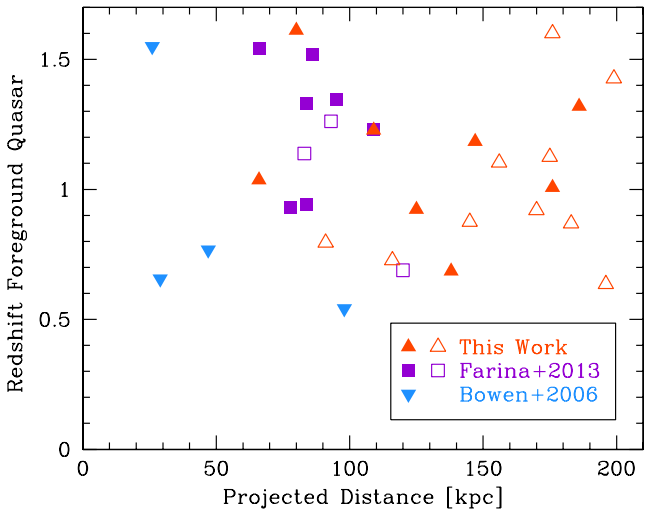

Figure 1. Distribution of observed projected quasar pairs in the redshift–impact parameter plane. Orange and cyan triangles and violet squares are targets from this work, Bowen et al. (2006), and Farina et al. (2013), respectively. Systems showing an absorption feature associated with the foreground quasar are highlighted with filled points.

Appenzeller et al. 1998) installed on the Antu Very Large Telescope (VLT) of the European Southern Observatory (ESO). This system is part of the sample of south quasar pairs we have investigated in Farina et al. (2013).

In Table 1 and Fig. 1, we present the general properties of the 18 observed pairs. These are radio-quiet quasars, with an average angular separation $\langle\Delta\theta\rangle \sim 18.6$ arcsec that corresponds to an average projected distance $\langle$pd$\rangle \sim 146$ kpc. These data represent a substantial increase in the number of pairs investigated so far, especially at separations larger than 100 kpc (see Fig. 1). Combined with data from Bowen et al. (2006) and Farina et al. (2013), our sample yields constraints on the physical properties of the Mg II absorbing gas surrounding quasars on scales between 26 and 200 kpc at an average redshift $\langle z\rangle \sim 1.1$. We stress that in the selection of the targets, we did not take into account for the possible presence of absorbers a priori; hence, our sample seems well suited to estimate the unbiased frequency of Mg II absorption systems associated with quasars.

3 OBSERVATIONS AND DATA ANALYSIS

Observations were carried out with the OSIRIS R2500R and R2500V grisms, yielding a spectral resolution of $R = \lambda/\Delta\lambda \sim 2500$ (with the 1 arcsec slit). This corresponds to a resolution element of FWHM $\sim 120\,\mathrm{km\,s^{-1}}$ that allows one to separate the doublet components but that is larger than the typical width of Mg II absorbers ($\lesssim$100 km s^{-1}; see e.g. Charlton & Churchill 1998). Thus, the internal dynamics of the absorption systems cannot be resolved. The position angle of the slit was oriented so that the spectrum of both the sources could be acquired simultaneously. The integration times range from 900 to 4800 s, depending on the magnitude of the background quasar. In order to correct for cosmic rays and for CCD cosmetic defects, for each target we have taken a series of three consecutive exposures, respectively, shifted by $\sim$5 arcsec. Details about the spectra gathered at ESO-VLT are given in Farina et al. (2013).

Standard IRAF[1] tools were used for the data reduction. The `ccdred` package was employed to perform bias subtraction, flat-field correction, image alignment, and combination. The spectra extraction, the background subtraction, and the calibrations both in wavelength and in flux were performed with `twod` and `oned` packages. Residuals of wavelength calibration are around 0.03 Å (sub-pixel). Standard stars' spectra were collected during the same nights of the targets. The absolute calibration of the spectra was obtained through the photometry of field stars present in *r*-band short exposures of the targets. This procedure yields a photometric accuracy of $\sim$0.1 mag (see Decarli et al. 2008, for details). The Galactic extinction was taken into account considering the estimates of Schlegel, Finkbeiner & Davis (1998) and assuming a standard interstellar extinction curve ($R_V = 3.1$; e.g. Cardelli, Clayton & Mathis 1989). The spectra of the quasar pairs are reproduced in Fig. 2.

4 ABSORPTION SYSTEMS ASSOCIATED WITH QUASARS

To investigate the presence of Mg II absorption lines in our spectra, we adopted the procedure described in Farina et al. (2013). In summary, we first model the quasar emission by interpolating with a cubic spline the median values of the flux estimated in bins of 20 Å each (e.g. Sbarufatti et al. 2005). Then, the 1σ detection limit of a spectral line was calculated from the equivalent width and the relative uncertainty of an unresolved absorption feature, assuming that it has the shape of a Gaussian with full width at half-maximum (FWHM) equal to the spectral resolution (see Schneider et al. 1993). Finally, the properties of the absorption features detected above a 3σ threshold were measured by fitting the lines with a single Gaussian function (e.g. Churchill et al. 2000). Uncertainties on the derived quantities were estimated through standard error propagation, and are dominated by the noise of the continuum close to the absorption lines.

Hereafter, we will refer to an absorber as *transverse* or as *line of sight* (LOS) depending on whether it was detected in the QSO$_B$ or in the QSO$_F$ spectrum. A detected absorption system will be considered as *associated* with the QSO$_F$ if it lies within $\pm$1000 km s^{-1} from the redshift derived from Mg II broad emission line (see Table 1). This operational definition was motivated by the large uncertainties associated with the fit of the broad lines and by the possibility that redshifts derived from various emission lines may differ from the systemic redshift by even hundreds of km s^{-1} (e.g. Tytler & Fan 1992; Richards et al. 2002; Bonning, Shields & Salviander 2007), and that LOS absorbers within up to thousands of km s^{-1} from a quasar may be still connected with the quasar itself (e.g. Wild et al. 2008; Shen & Ménard 2012). A choice of a wider velocity range to associate the LOS absorption systems to QSO$_F$ has only marginal effects on our results (see Section 5).

In our new sample, we detected eight Mg II transverse absorption features associated with the QSO$_F$ (almost doubling the number of known such system,; see Bowen et al. 2006; Farina et al. 2013), while no associated absorbers are present along the LOS (see Table 2 and Fig. 3). The average shift between transverse absorbers and Mg II broad line is $\langle\Delta V_{\mathrm{QSO-Abs.}}\rangle \sim -250\,\mathrm{km\,s^{-1}}$ with an rms of $\sim$380 km s^{-1} confirming the strict association with the quasars. This

[1] IRAF (Tody 1986) is distributed by the National Optical Astronomy Observatories, which are operated by the Association of Universities for Research in Astronomy, Inc., under cooperative agreement with the National Science Foundation.

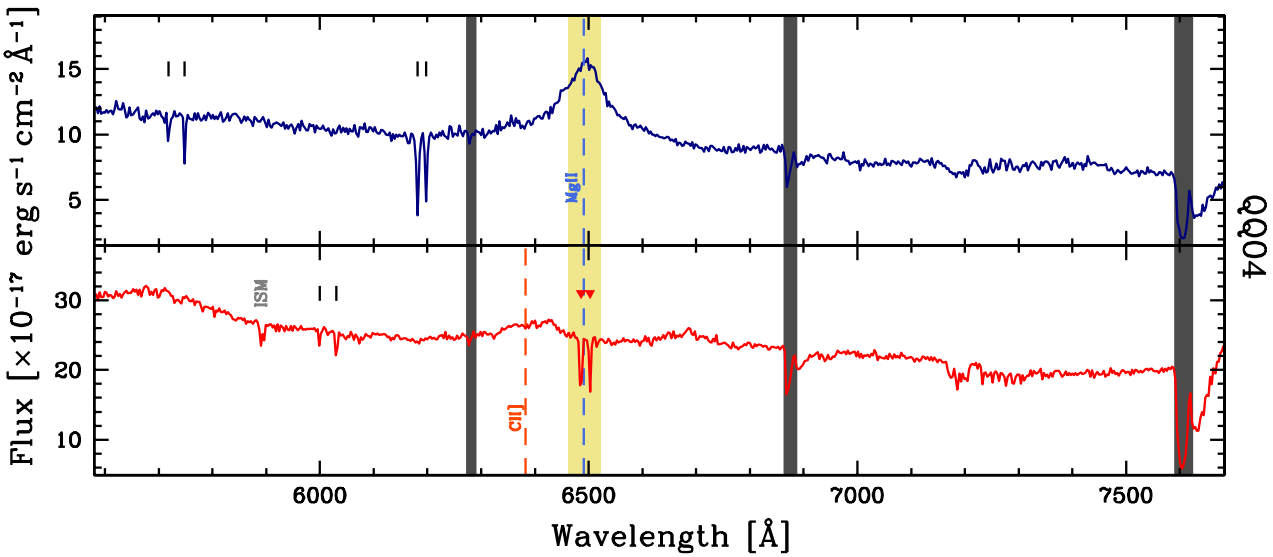

Figure 2. Spectra of the projected quasar pair QQ04 corrected for Galactic extinction and binned by 3 pixel. Blue and red solid lines refer to QSO_F and to QSO_B, respectively. Main quasar emission lines and Galactic absorption are labelled. The shaded yellow region marks the wavelength range considered to associate an Mg II doublet to the QSO_F (see Section 4) and dark grey bars cover regions affected by prominent telluric absorptions. Black ticks point to absorption lines detected over a 3σ threshold (see Appendix B) and red triangles highlight the Mg II absorption doublet associated with the QSO_F (see Table 2). Figures of the other quasar pairs are available in the electronic edition of the journal as Supporting Information.

Table 2. Properties of Mg II absorption features associated with QSO_F: our identification label of the quasar (ID), observed wavelength (λ_{abs}), rest-frame equivalent width (W_r), doublet ratio (DR), and redshift (z_{abs}). If no absorption system is present, the 2σ upper limit for the W_r is quoted. The labels F and B indicate the foreground and the background quasar, respectively.

ID	$\lambda_{abs}(\lambda2796)$ (Å)	$W_r(\lambda2796)$ (Å)	$\lambda_{abs}(\lambda2803)$ (Å)	$W_r(\lambda2803)$ (Å)	DR	z_{abs}
QQ01F	–	<0.22	–	<0.22	–	–
QQ01B	–	<0.13	–	<0.13	–	–
QQ02F	–	<0.17	–	<0.17	–	–
QQ02B	7329.1	0.92 ± 0.10	7347.7	0.98 ± 0.09	0.94 ± 0.12	1.6213 ± 0.0001
QQ03F	–	<0.12	–	<0.12	–	–
QQ03B	–	<0.15	–	<0.15	–	–
QQ04F	–	<0.12	–	<0.12	–	–
QQ04B	6485.8	0.78 ± 0.03	6502.5	0.58 ± 0.02	1.34 ± 0.04	1.3197 ± 0.0001
QQ05F	–	<0.21	–	<0.21	–	–
QQ05B	5615.2	0.50 ± 0.06	5624.8	0.39 ± 0.05	1.29 ± 0.19	1.0075 ± 0.0008
QQ06F	–	<0.22	–	<0.22	–	–
QQ06B	5379.1	0.39 ± 0.07	5392.7	0.28 ± 0.08	1.41 ± 0.12	0.9239 ± 0.0001
QQ07F	–	<0.17	–	<0.17	–	–
QQ07B	–	<0.14	–	<0.14	–	–
QQ08F	–	<0.19	–	<0.19	–	–
QQ08B	4711.2	0.33 ± 0.04	4724.0	0.24 ± 0.03	1.37 ± 0.19	0.6852 ± 0.0002
QQ09F	–	<0.17	–	<0.17	–	–
QQ09B	5691.9	0.72 ± 0.05	5706.5	0.42 ± 0.03	1.71 ± 0.14	1.0358 ± 0.0001
QQ10F	–	<0.22	–	<0.22	–	–
QQ10B	–	<0.17	–	<0.17	–	–
QQ11F	–	<0.16	–	<0.16	–	–
QQ11B	–	<0.24	–	<0.24	–	–
QQ12F	–	<0.21	–	<0.21	–	–
QQ12B	6136.2	0.64 ± 0.07	6152.0	0.47 ± 0.06	1.36 ± 0.19	1.1947 ± 0.0001
QQ13F	–	<0.17	–	<0.17	–	–
QQ13B	–	<0.11	–	<0.11	–	–
QQ14F	–	<0.17	–	<0.17	–	–
QQ14B	–	<0.11	–	<0.11	–	–
QQ15F	–	<0.18	–	<0.18	–	–
QQ15B	–	<0.14	–	<0.14	–	–
QQ16F	–	<0.13	–	<0.13	–	–

Table 2 – *continued*

ID	$\lambda_{abs}(\lambda2796)$ (Å)	$W_r(\lambda2796)$ (Å)	$\lambda_{abs}(\lambda2803)$ (Å)	$W_r(\lambda2803)$ (Å)	DR	z_{abs}
QQ16B	6233.6	0.91 ± 0.04	6249.7	0.61 ± 0.04	1.51 ± 0.11	1.2296 ± 0.0001
QQ17F	–	<0.21	–	<0.21	–	–
QQ17B	–	<0.22	–	<0.22	–	–
QQ18F	–	<0.13	–	<0.13	–	–
QQ18B	–	<0.11	–	<0.11	–	–

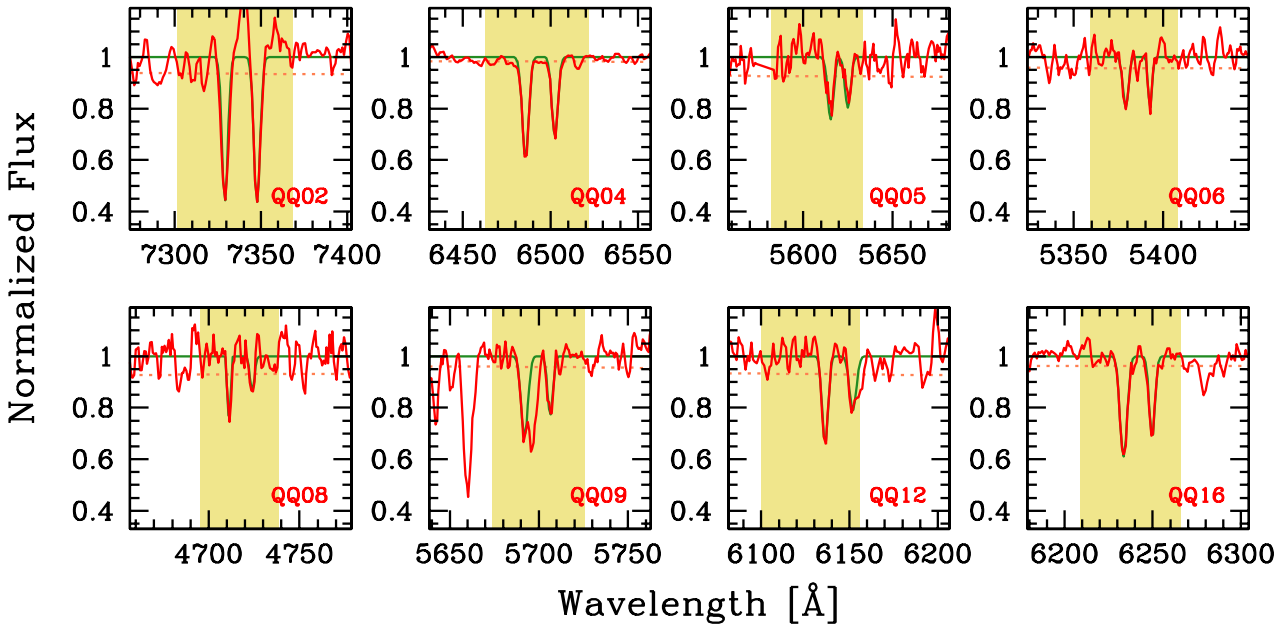

Figure 3. Close-up of the normalized QSO_B spectra where the transverse absorption systems are detected (red line). The Gaussian fit performed as described in Section 4 and in Farina et al. (2013) is marked with a green solid line, and the $1-1\sigma$ spectrum with a pale-red dotted line. The shaded yellow region shows the windows in which we consider the absorption system as associated with QSO_F. The system QQ08 exhibit several strong absorption systems close to the Mg II doublet that are not associated with QSO_F (see Appendix B).

is further supported by the paucity of random absorbers present in the proximity of quasars. Indeed, integrating over 2000 km s^{-1}the redshift number density of systems with $W_r(\lambda2796) \geq 0.30$ Å, only ∼0.01 absorption systems are expected (Nestor, Turnshek & Rao 2005). These results exclude that the observed Mg II lines are due to chance effect. The rest-frame equivalent width of the observed transverse absorption systems range from $W_r(\lambda2796) = 0.33$ to 0.92 Å with an average $W_r(\lambda2796)/W_r(\lambda2803)$ doublet ratio of $\langle DR \rangle = 1.35 \pm 0.03$. This suggests that most of our systems are partially saturated as commonly observed in intervening Mg II doublets detected in quasar spectra (e.g. Nestor et al. 2005). The absence of LOS Mg II absorbers agrees with the studies performed by Vanden Berk et al. (2008) and Shen & Ménard (2012) on SDSS spectra, which have shown that LOS Mg II absorbers occur only in a few per cent of the examined systems, and that are possibly related to an enhanced star formation rate of the quasar host galaxy.

5 DISCUSSION

In this section, we report on the detected Mg II absorption systems and relate their properties to the impact parameters, the mass of the host galaxies, and the direction of view (i.e. transverse or LOS). We also compare our results with the properties of the CGM of normal galaxies, for which Mg II absorption systems were detected up to pd ∼ 200 kpc (e.g. Bergeron & Boissé 1991; Steidel et al. 1997; Kacprzak et al. 2008; Chen et al. 2010a; Nielsen et al. 2013a, and references therein). In particular, we investigate whether galaxies and quasars show different trend in the well-known anticorrelation between $W_r(\lambda2796)$ and the impact parameter (e.g. Lanzetta & Bowen 1990; Steidel & Sargent 1992; Steidel 1995).

5.1 Covering fraction

To study the covering fraction (f_C) of Mg II absorption systems at different impact parameters from the quasar, we define $f_C \equiv f_C(W_{lim})$ as the fraction of absorbers with W_r greater than a given equivalent width (W_{lim}) detected in each bin of projected distance. If the upper limit on the equivalent width of an absorber (see Table 2) is larger than W_{lim}, this system is not considered in the estimate. The 1σ uncertainties in f_C are calculated upon the binomial statistics (e.g. Gehrels 1986; Cameron 2011).

In Fig. 4, we plot f_C of Mg II transverse absorbers associated with quasars against the impact parameter, including data from Bowen et al. (2006) and Farina et al. (2013). The covering fraction of absorbers with $W_r(\lambda2796) \geq 0.30$ Å is $f_C(0.30\,\text{Å}) = 1.00^{+0.00}_{-0.47}$ in the first bin (20 kpc < pd ≤ 65 kpc) and smoothly decreases with the impact parameter down to $f_C(0.30\,\text{Å}) = 0.22^{+0.24}_{-0.12}$ at 155 kpc < pd ≤ 200 kpc. In our sample, 10 Mg II absorbers have

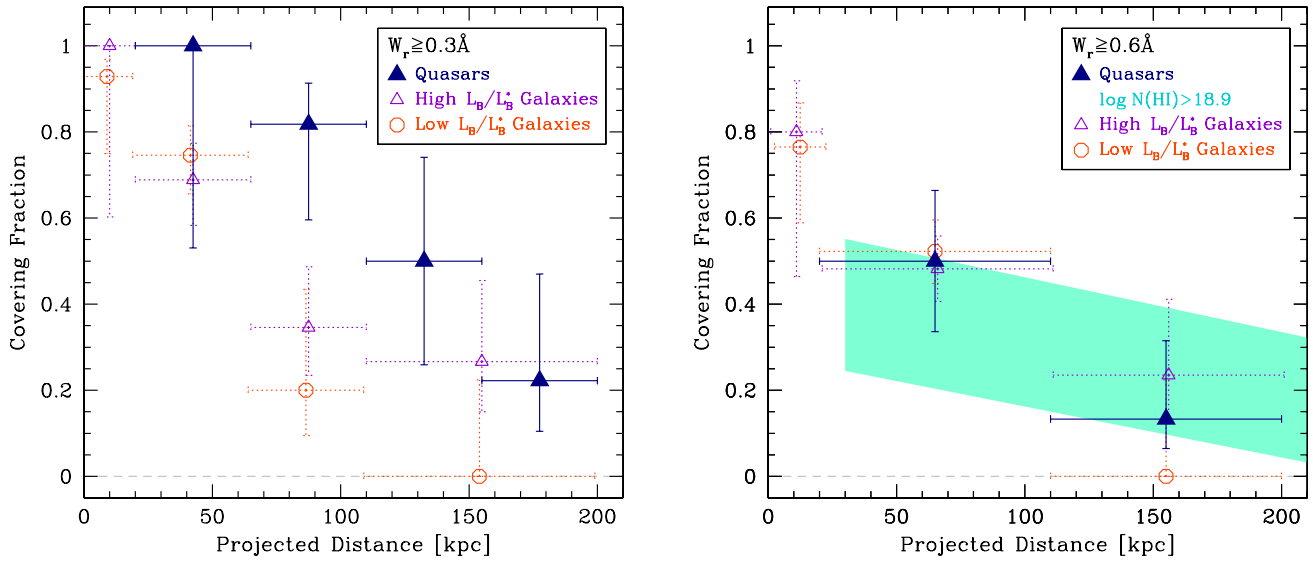

Figure 4. Left-hand panel: covering fraction profile for transverse absorption systems with $W_r(\lambda2796) > 0.30$ Å associated with QSO_F (blue triangles). The horizontal bars indicate the impact parameter bin width and vertical bars are the 1σ binomial uncertainties (e.g. Gehrels 1986; Cameron 2011). For comparison, we plot also the Mg II covering fraction of 182 isolated (i.e. without a companion closer than 100 kpc and 500 km s^{-1}) galaxies investigated by Nielsen et al. (2013b) with B-band luminosities larger (violet empty triangles) and smaller (orange empty circles) than $L_B \sim 0.6\,L_B^\star$, where $L_B^\star$ is the characteristic luminosity of galaxies as derived from Faber et al. (2007). We converted the upper limits listed in Nielsen et al. (2013b) to the 2σ limits considered here. Right-hand panel: same as left-hand panel but for absorption systems with $W_r(\lambda2796) > 0.6$ Å. We also show the $\pm1\sigma$ region of the covering fraction of the H I absorbers associated with high-redshift quasars ($1.6 \lesssim z \lesssim 3.2$) presented by Prochaska et al. (2013a, pale blue filled area). For the sake of comparison, we limit the H I column density to $N_{\rm H\,I} \gtrsim 10^{18.9}$ cm^{-2} that roughly corresponds to the considered Mg II equivalent width limit (see text for details).

$W_r(\lambda2796) \geq 0.60$ Å; the covering fraction of these systems is $f_C(0.60\,\text{Å}) = 0.50^{+0.16}_{-0.16}$ between 20 and 110 kpc and $f_C(0.60\,\text{Å}) = 0.13^{+0.18}_{-0.07}$ in the 110–200 kpc bin.

Various studies on the incidence of Mg II absorbers agree that the number of such systems increase in the proximity of a galaxy. However, the derived covering fractions span a broad range of values (i.e. from ∼0.2 to ∼1) depending on the diverse sets of explored galaxy properties, impact parameter, and equivalent width limit (e.g. Bechtold & Ellingson 1992; Tripp & Bowen 2005; Barton & Cooke 2009; Gauthier, Chen & Tinker 2010; Lovegrove & Simcoe 2011; Lundgren et al. 2012). In order to minimize the possible bias towards a specific galaxy population, we will assume as reference the recent estimates of Nielsen et al. (2013b), derived from a large and heterogeneous compilation of 182 isolated galaxies at redshift $0.1 \lesssim z \lesssim 1.1$ with B-band magnitudes varying from $M_B = -16.1$ to -23.1 (Nielsen et al. 2013a, and references therein). The quoted 3σ upper limits in the detection of $W_r(\lambda2796)$ were converted to the 2σ limit considered in this work.

We note that, quasars in each bin show, on average, a higher $f_C(0.30\,\text{Å})$ with respect to galaxies. In particular, while *low-luminosity* galaxies (defined by Nielsen et al. as galaxies with B-band luminosity $L_B/L_B^\star \lesssim 0.6$) do not reveal any absorption systems at impact parameter larger than 110 kpc, *high-luminosity* galaxies ($L_B/L_B^\star \gtrsim 0.6$) show a behaviour more similar to quasars, with a CGM extending also at large separations (see left-hand panel of Fig. 4). The difference between the covering fraction at different impact parameters of quasars, and of high– and low-luminosity galaxies almost disappears for systems with $W_r(\lambda2796) \geq 0.6$ Å (see right-hand panel of Fig. 4). Since quasars are hosted by luminous galaxies that in some cases show an excess of blue light (e.g. Bahcall et al. 1997; Floyd et al. 2013; Kotilainen et al. 2013; Falomo et al. 2014), our results are qualitatively in agreement with a luminosity dependence for the covering fraction of Mg II absorbing gas with $W_r \geq 0.3$ Å (e.g. Nielsen et al. 2013b, and references therein).

It is of interest to compare our results with the H I covering fraction observed in high-redshift quasars by Prochaska et al. (2013a), who investigate a sample of 74 close projected quasar pairs with projected separations pd < 300 kpc and average redshift $\langle z \rangle \sim 2.2$. We convert the Mg II equivalent width limit into an H I column density ($N_{\rm H\,I}$) with the empirical relation provided by Ménard & Chelouche (2009)[2] and derived from the sample of low-redshift Lyman absorbers of Rao et al. (2006). Within ∼100 kpc, the H I covering fraction is $f_C\,(\text{H I}) \sim 0.33$ for absorbers with $N_{\rm H\,I} > 10^{18.9}$ cm^{-2} (roughly corresponding to $W_r(\lambda2796) > 0.60$ Å) that is lower, but still consistent within uncertainties, than the $f_C(0.60\,\text{Å}) \sim 0.50$ we found for lower redshift quasars. This suggests that the CGM of quasars does not evolve significatively from redshift $z \sim 2$ to ∼1 (see also Chen 2012; Fumagalli et al. 2013). This result could be influenced by the large scatter present in the $W_r(\lambda2796)$ versus $N_{\rm H\,I}$ plane. Column densities of $N_{\rm H\,I} \sim 10^{18.5}$ cm^{-2} could still be associated with $W_r(\lambda2796) \sim 0.6$ Å absorption systems, suggesting that we are most probably underestimating the Mg II covering fraction associated with $z \sim 2$ quasars. Future direct observations of the Mg II absorbing gas associated with high-redshift quasars are thus needed to give further support to this result.

5.2 $W_r(\lambda2797)$ and impact parameter

It is well assessed that the equivalent width of Mg II absorption features anticorrelates with the impact parameter (e.g. Lanzetta & Bowen 1990; Bergeron & Boissé 1991; Steidel 1995; Chen et al. 2010a; Nielsen et al. 2013b). In Fig. 5, we present the distribution

[2] We considered the relation between median $N_{\rm H\,I}$ and $W_r(\lambda2796)$.

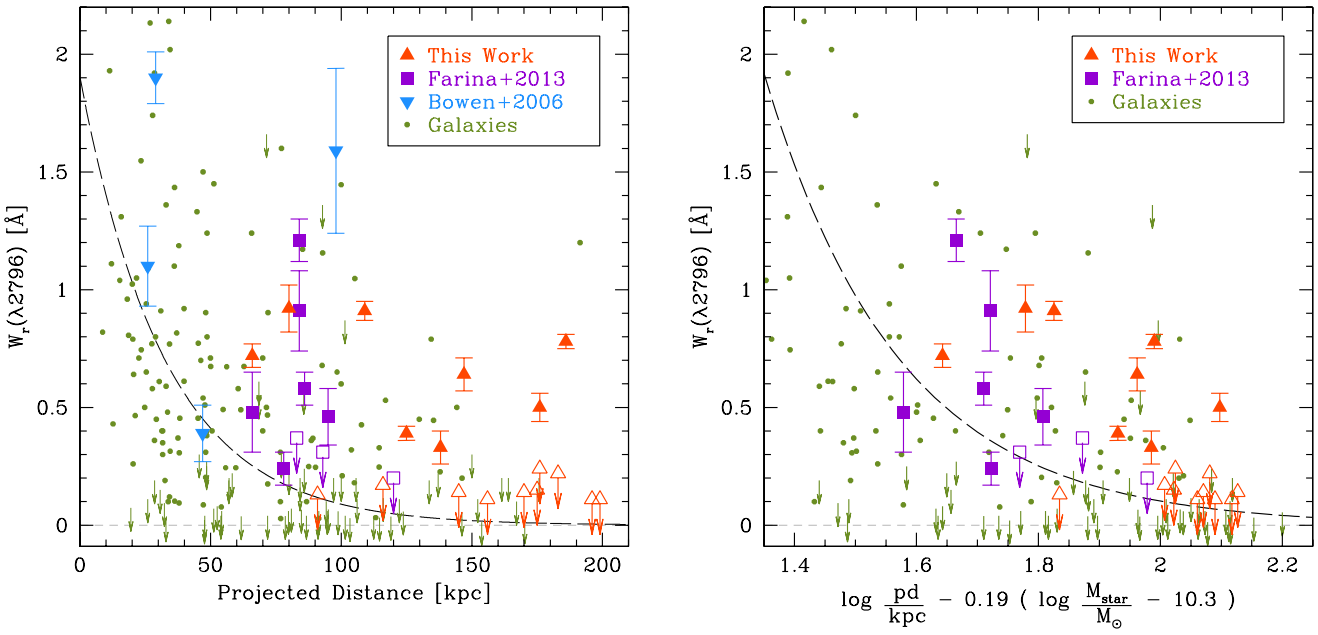

Figure 5. Left-hand panel: rest-frame equivalent width of Mg II(λ2796) absorption line as a function of projected distance. Orange and cyan filled triangles and violet filled squares represent quasars in which an associated transverse absorption system is detected, while the empty ones are 2σ upper limits (data are from this work, Bowen et al. 2006, and Farina et al. 2013, respectively). Green points and arrows are absorption features associated with galaxies and upper limits from Werk et al. (2013), Gauthier & Chen (2011), Kacprzak et al. (2011), Chen et al. (2010a, also including the absorption detected in *group galaxies*), and Barton & Cooke (2009). Black dashed line shows the best fit of the anticorrelation proposed by Nielsen et al. (2013b). For the sake of comparison, the upper limits listed by Barton & Cooke (2009) were converted to the considered 2σ limits, and all the data were rescaled to the considered cosmological model. Right-hand panel: rest-frame equivalent width of Mg II(λ2796) absorption line as a function of projected distance and stellar mass for quasars and galaxies. Orange triangles and violet squares are data for quasars from this work and Farina et al. (2013), respectively, while green points and arrows are absorption features associated with galaxies and upper limits from Werk et al. (2013), Chen et al. (2010b), and Barton & Cooke (2009). Spectra of the four QSO_F in Bowen et al. (2006) are not publicly available and thus we cannot give an estimate of the M_{host} for these systems. Black dashed line is the W_r versus pd anticorrelation for galaxies including the scaling relation with stellar mass proposed by Chen et al. (2010b). For the *x*-axis, we have adopted the same projection of fig. 3 in Chen et al. (2010b).

of $W_r(\lambda2796)$ as a function of pd for quasars and for galaxies derived from Barton & Cooke (2009), Chen et al. (2010a), Kacprzak et al. (2011), Gauthier & Chen (2011), and Werk et al. (2013). While some of the absorbers associated with quasars lie almost in the same regions of the case of galaxies, at impact parameters larger than ∼50 kpc a number of systems with $W_r(\lambda2796) \gtrsim 0.5$ Å are present. These are rarely found in correspondence of galaxies (see also Farina et al. 2013). In order to test this qualitative finding, we performed a non-parametric Kendall's test that include upper limits (e.g. Isobe, Feigelson & Nelson 1986). While for galaxies $W_r(\lambda2796)$ and pd are anticorrelated at the 7.9σ level (Nielsen et al. 2013b, see also, e.g. Chen et al. 2010a), for quasar the significance level is much weaker (2.2σ). In addition, a two-dimensional Kolmogorov–Smirnov test (Fasano & Franceschini 1987) performed on the sources with detected Mg II absorption, ruled out with a probability of $P_{2D-KS} = 99.8$ per cent the null hypothesis that, in the 20 kpc < pd ≤ 200 kpc region, the absorption systems associated with galaxies and to quasars are drawn from the same parent population.

5.3 The role of the mass of galaxies

Quasars are generally harboured by massive galaxies with a typical mass of few times 10^{11} $M_\odot$ (McLure et al. 1999; Falomo, Kotilainen & Treves 2001; Kukula et al. 2001; Falomo et al. 2004, 2008; Jahnke & Wisotzki 2003; Floyd et al. 2004, 2013; Hyvönen et al. 2007; Kotilainen et al. 2007, 2009, 2013); hence, the stellar mass (considered as an optimal proxy for the dark halo masses, e.g. Moster et al. 2010; More et al. 2011) should have a substantial role in shaping the W_r−pd anticorrelation (e.g. Chelouche et al. 2008; Chen & Tinker 2008).

No deep images of the considered systems are available to directly detect the quasar host galaxies. Therefore, we derive an estimate of the mass (M_{host}) from the M_{BH}−M_{host} relation (see e.g. Marconi & Hunt 2003; Häring & Rix 2004; Peng et al. 2006a,b; Decarli et al. 2010b, 2012; Bennert et al. 2011). In particular, we consider the relation presented by Decarli et al. (2010b), which is based upon the study 96 quasars in the redshift range $0.07 < z < 2.74$:

$$\log \frac{M_{BH}}{M_{host}} = (0.28 \pm 0.06)\, z - (2.91 \pm 0.06)\,, \qquad (1)$$

where M_{BH} is the black hole mass deduced with the virial method as described in Appendix A, and z is the redshift of the foreground quasar. Uncertainties associated with the M_{host} obtained in this way could be as large as ∼0.6 dex (e.g. Decarli et al. 2010b). We note that Decarli et al. (2010b) estimated the stellar masses assuming bulge-dominated host galaxies and a passive evolution of the stellar population from $z = 5$ to 0. Various authors showed that quasars often suffer of intense star formation episodes during their lifetime (e.g. Canalizo & Stockton 2013) and thus masses calculated from equation 1 (see Table 1) could be underestimated.

In the right-hand panel of Fig. 5, we show the distribution of the $W_r(\lambda2796)$ as a function of the impact parameter, rescaled for the stellar mass for galaxies from Barton & Cooke (2009),

Chen et al. (2010b), and Werk et al. (2013), on average, $M_{\rm gal} = 0.4 \times 10^{11}\,{\rm M}_{\odot}$, and for the quasar hosts (on average, $M_{\rm host} \sim 2.0 \times 10^{11}\,{\rm M}_{\odot}$) assuming, for the sake of comparison, the same scale on the x-axis presented in Chen et al. (2010b):

$$\mathrm{pd_M} = \log \frac{\mathrm{pd}}{\mathrm{kpc}} - 0.19 \left(\log \frac{M_{\rm star}}{\mathrm{M}_{\odot}} - 10.3 \right). \quad (2)$$

Taking into account the mass of the galaxies, the anticorrelation between $W_{\rm r}$ and pd for quasars is enhanced to the 3.1σ level[3] and the null hypothesis of a same parent population for absorption systems associated with quasars and galaxies is ruled out with a probability of $P_{\rm 2D\text{-}KS} = 77.4$ per cent. The $\widetilde{\chi}^2$ values for our data calculated against the relations presented by Nielsen et al. (2013b) and Chen et al. (2010b, see Fig. 5) prior and after considering the host galaxy masses decrease by ∼30 per cent.

In Fig. 6, we show the Mg II covering fraction of quasars and galaxies estimated in bins of $\mathrm{pd_M}$. In spite of the large uncertainties, quasars show a systematically higher covering fraction than galaxies. This difference is more marked for systems with $W_{\rm r}(\lambda2796) > 0.3$ Å, but holds also for those with $W_{\rm r}(\lambda2796) > 0.6$ Å.

These findings suggest that the stellar mass plays an important role, but its effect is not strong enough to reconcile the different properties of the CGM of galaxies and of quasars. As suggested by different studies, other parameters related to the host galaxies could be involved, such as: star formation, morphology, or close galactic environment (e.g. Kacprzak et al. 2007; Chen et al. 2010a,b; Bordoloi et al. 2011, 2012; Ménard et al. 2011; Kacprzak, Churchill & Nielsen 2012, and next section). Moreover, the *patchiness* of the cool gas in the CGM could have an important effect in the large scatter present in the anticorrelation (e.g. Kacprzak et al. 2008).

Our results are qualitatively in agreement with the systematic segregation of the galaxy virial masses on the $W_{\rm r}(\lambda2796)$–pd recently reported by Churchill et al. (2013a,b): galaxies with higher mass haloes show stronger Mg II absorption systems at a given pd with respect to lower mass haloes. In this context, it is of interest to compare our findings with the sample of Mg II absorbers observed by Gauthier & Chen (2011) around luminous red galaxies (LRGs), which are expected to inhabit haloes with masses comparable or larger than those of quasars (e.g. Zheng et al. 2009). Between 45 and 200 kpc (where the separation limit of 45 kpc is set by the smallest impact parameter investigated by Gauthier & Chen 2011), we calculate a covering fraction of $f_{\rm C}(0.3\,\text{Å}) = 0.42^{+0.20}_{-0.16}$ for LRGs that is slightly lower but consistent within the uncertainties with the $f_{\rm C}(0.3\,\text{Å}) = 0.59^{+0.12}_{-0.13}$ observed for quasars.

5.4 The role of the immediate galactic environment

Since quasars are often associated with group of galaxies (e.g. Wold et al. 2001; Serber et al. 2006; Hutchings et al. 2009), it is of interest to estimate the contribution of the immediate galactic environment to the strength of the observed absorption systems. Indeed, the presence of a rich environment could induce an overabundance of strong equivalent width systems ($W_{\rm r}(\lambda2796) > 1$ Å) compared to field galaxies (e.g. Nestor et al. 2007; Lopez et al. 2008; Kacprzak, Murphy & Churchill 2010; Andrews et al. 2013; Gauthier 2013).

[3] A Monte Carlo analysis of the anticorrelation shows that, even allowing the host galaxy masses to vary by 0.6 dex around the calculated values, the significance is increased (i.e. it is better than 2.2σ) in more than 70 per cent of the realizations. The large uncertainties associated with the stellar mass of the quasar hosts marginally affect this result.

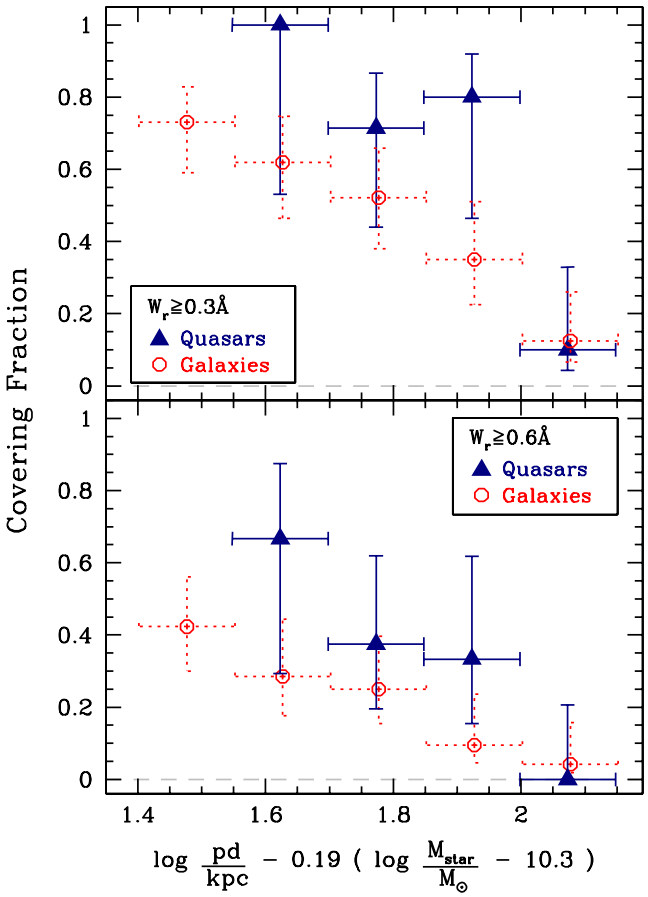

Figure 6. Top panel: covering fraction profile for transverse absorption systems with $W_{\rm r}(\lambda2796) > 0.30$ Å associated with $\mathrm{QSO_F}$ (blue filled triangles) with impact parameter normalized by the host galaxy masses as in Fig. 5. We also show the Mg II covering fraction of galaxies (red empty circles) with public available measure of the stellar masses from Chen et al. (2010b), Barton & Cooke (2009), and Werk et al. (2013) that constitute a representative sub-sample of roughly half the systems studied by Nielsen et al. (2013b). Error bars are calculated as in Fig. 4. Bottom panel: same as the top panel but for absorption systems with $W_{\rm r}(\lambda2796) > 0.6$ Å.

In order to evaluate this effect, we have first simulated the typical galactic environment of a quasar following the quasar–galaxy cross-correlation function presented by Zhang et al. (2013). Then, to each mock galaxy we have assigned a CGM that reproduce the observed properties of the Mg II absorption systems reported by Chen et al. (2010a) and Nielsen et al. (2013a). Finally, the average effect of the environment in terms of strength of the absorption and covering fraction was calculated summing up the contribution of the single galaxies at different impact parameter from the quasar. A detailed description of the simulation and a discussion of the possible caveats in our estimate are given in Appendix C. We here summarize our results: (i) less than 25 per cent of the quasar sight lines are covered by the absorbing gas associated with companion galaxies; (ii) the covering fractions of the absorbing gas associated with the quasar's environment show an almost flat profile between 20 and 200 kpc with $f_{\rm C,Env}(0.30\,\text{Å}) \sim 0.10$ and $f_{\rm C,Env}(0.60\,\text{Å}) \sim 0.05$; and (iii) the contribution of galaxies in proximity of quasars to the strength of the observed absorption systems is $W_{\rm r,Env}(\lambda2796) \lesssim 0.1$ Å, with almost no dependence on the impact parameter. This latter effect is of the same order of magnitude of the uncertainties in the $W_{\rm r}(\lambda2796)$ measurements, thus has a marginal impact on our results, especially

for the systems with large W_r. The contribution of the environment to the covering fraction is also negligible; however, we notice that at large impact parameter (and small f_C) the presence of satellite galaxies could have enhanced the measured f_C up to a factor of 2 (see Fig. 4).

5.5 Fe II transverse absorption systems

In 21 of the investigated quasar pairs, the spectral coverage of our data allows us to investigate also for the presence of the Fe II λλ2586, 2600 absorption systems. We detect four Fe II(λ2600) absorption lines (see Fig. 7 and Table B1), formally yielding a covering fraction of $f_C\,(\mathrm{Fe\,II}) = 0.19^{+0.15}_{-0.08}$ for systems with $W_r(\lambda2600) \geq 0.30$Å and pd ≤ 200 kpc.

It is worth noting that absorption systems with $W_r(\lambda2796) \geq 0.50$ Å and $W_r(\lambda2600)/W_r(\lambda2796) > 0.5$ have an ∼40 per cent probability to be a damped Lyα systems (DLAs) with $N_{\mathrm{H\,I}} > 10^{20}$ cm^{-2} (Rao et al. 2006). Only two of the detected Mg II absorptions match these constraints (see Fig. 7), suggesting that also the stronger absorptions might not arise in galactic disc, where high column densities are expected (e.g. Zwaan et al. 2005). However, we cannot exclude the possibility that the Mg II absorption originate from extraplanar neutral gas associated with spiral galaxies (see Sancisi et al. 2008, and references therein).

The estimated fraction of DLAs present within 200 kpc from $z \sim 1.1$ quasars (i.e. 4^{+5}_{-2} per cent) is consistent with the 10^{+8}_{-4} per cent observed at higher redshift by Prochaska et al. (2013a). This further supports the hypothesis of little, if any, evolution of the quasars' CGM.

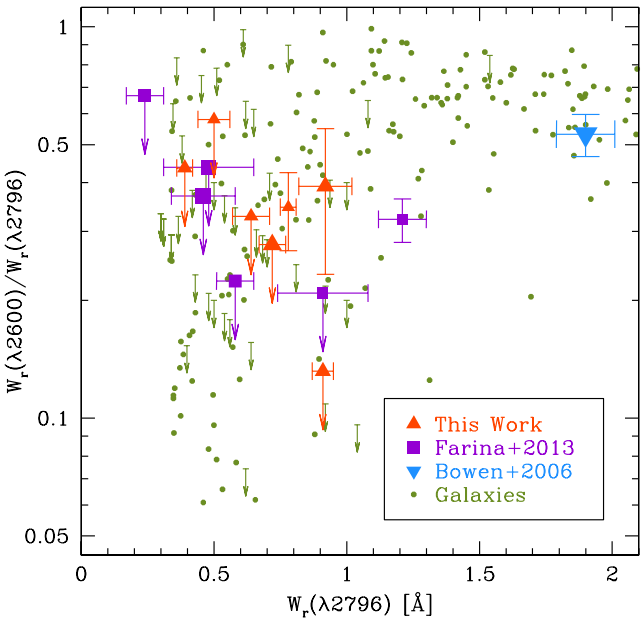

Figure 7. Ratio of the rest-frame equivalent width of Fe II(λ2600) to Mg II(λ2796) absorption lines as a function of $W_r(\lambda2796)$. Symbols are equivalent to those in Fig. 5. Only quasars that shows the presence of an associated Mg II transverse absorption systems are shown and the size of these points is inversely proportional to the logarithm of the impact parameter. Note that Bowen et al. (2006) report information about the presence of Fe II associated absorption line only for the quasar SDSS J083649.45+484150.0, which is one of the closer pair considered here (pd = 29 kpc). Data for galaxies are from the sample of 87 Mg II absorption systems with $W_r(\lambda2796) > 0.3$ Å investigated by Rodríguez Hidalgo et al. (2012) in the redshift range $0.2 < z < 2.5$ and from the study of 197 Mg II absorption features associated with DLAs at $z < 1.65$ performed by Rao et al. (2006).

5.6 Anisotropic distribution of Mg II absorbers

In the whole sample of quasars, we do not detect any LOS Mg II absorption lines of the same strength of the transverse one. We emphasize that even considering a larger velocity window to associate the LOS absorbers to the quasars (e.g. <5000 km s^{-1} as suggested by Sharma, Nath & Chand 2013), only one more systems would be added to our sample (see Appendix B). A similar behaviour was also observed for H I absorptions systems (e.g Hennawi & Prochaska 2007), while C IV LOS absorbers were detected in two out of the three quasars investigated by Farina et al. (2013). This higher incidence of C IV LOS absorbers with respect to Mg II is in agreement with the study of Wild et al. (2008) in their SDSS-based study of LOS absorption systems directly associated with quasars.

The absence of LOS absorbers is possibly a consequence of the SMBH emission, which could photoionize the surrounding Mg II absorbing clouds. Chelouche et al. (2008) consider that the CGM of quasars is clumpy and filled by clouds having a size of ∼1 pc and a density of $\sim 10^{-2}$ cm^{-3} (see Petitjean & Bergeron 1990; Churchill & Vogt 2001; Rauch et al. 2002; Churchill, Vogt & Charlton 2003; Ellison et al. 2004; Prochaska & Hennawi 2009). Under these conditions, a quasar with luminosity $\sim 10^{46}$ erg s^{-1} (the average of our sample, see Table 1 and Farina et al. 2013) is able to photoionize the gas of the CGM and to heat it (through photoabsorption) up to a temperature of $T \sim 10^5$ K, allowing the persistence of only few Mg II absorption systems. This is in agreement with Wild et al. (2008), who found that the SMBH emission photoionize Mg II absorbers with $W_r(\lambda2796) \geq 0.30$ Å out to at least 800 kpc, while, thanks to its higher ionizing potential, C IV absorbing clouds could survive.

In this scenario, the presence of the transverse Mg II absorption features is explained considering that the quasar radiation is emitted into cones (e.g. Antonucci 1993; Elvis 2000) and thus only marginally affects the gas in the transverse direction (e.g. Hennawi & Prochaska 2007; Bowen et al. 2006; Chelouche et al. 2008; Prochaska et al. 2013a,b). Similarly a non-isotropic emission of quasars is invoked to explain the non-detection of the transverse proximity effect (i.e. the expected decrease in absorption systems in the Lyα forest of close projected quasar pairs due to the ionizing emission of the foreground SMBH; see e.g. Crotts 1989; Dobrzycki & Bechtold 1991; Liske & Williger 2001; Schirber, Miralda-Escudé & McDonald 2004).

6 SUMMARY AND CONCLUSIONS

We have investigated the properties of the Mg II absorbing CGM of quasars using a sample of 31 projected quasars pairs with impact parameter ranging from 20 to 200 kpc at $0.5 \lesssim z \lesssim 1.6$.

The main results of our study are as follows.

(1) Quasars are surrounded by a large amount of Mg II absorbing gas with a covering fraction that ranges from $f_C \sim 1.0$ at pd $\lesssim 60$ kpc to $f_C \sim 0.2$ at pd $\gtrsim 150$ kpc for systems with $W_r(\lambda2796) > 0.3$ Å.

(2) We find a weak anticorrelation between the Mg II rest-frame equivalent width and the impact parameter that is enhanced once the stellar mass of the quasar host galaxy is taken into account.

(3) While Mg II absorbers are frequently observed in the transverse direction, such systems are rarely found along the LOS. This supports a scenario where the ionizing emission of the SMBH occurs in cones (e.g. Antonucci 1993); thus, the CGM is not

illuminated by the central engine in the transverse direction, resulting in a non-isotropic distribution of the absorption systems.

Since quasars are harboured by luminous galaxies, our result supports a scenario in which galaxies with high luminosity/mass typically possess a more extended CGM with respect to the fainter ones (e.g. Chelouche et al. 2008; Nielsen et al. 2013b). Nevertheless, we observe that quasars are surrounded by a larger amount of Mg II absorbing gas even considering the difference in size. The presence of this large reservoir of cool gas may be a challenge for the cold-mode accretion paradigm that predicts a little amount of cool gas around more massive haloes (e.g. Birnboim & Dekel 2003; Kereš et al. 2005, 2009; van de Voort & Schaye 2012; Nelson et al. 2013). Possibly wind outflows and/or inflows of metal-enriched gas associated with the galaxy interactions responsible for the quasar activity could be able to supply cool Mg II absorbing gas to the CGM. Future deep imaging observation of the foreground quasars aimed to characterize the quasar hosts and its close environment will help to clarify the origin of the Mg II absorption systems and to investigate which are the most important parameters that regulate the properties of the CGM of quasars.

ACKNOWLEDGEMENTS

We are grateful to E. Lusso and C. Montuori for useful discussion and helpful comments on the manuscript. We acknowledge financial contribution from the grant PRIN–MIUR 2010NHBSBE by the Italian Ministry of University and Research. EPF acknowledges funding through the ERC grant 'Cosmic Dawn'. Support for RD was provided by the DFG priority program 1573 'The physics of the interstellar medium'. This work was based on observations made with the GTC Telescope in Roque de los Muchachos and the ESO/VLT Telescope in Paranal. Funding for the SDSS and SDSS-II has been provided by the Alfred P. Sloan Foundation, the Participating Institutions, the National Science Foundation, the U.S. Department of Energy, the National Aeronautics and Space Administration, the Japanese Monbukagakusho, the Max Planck Society, and the Higher Education Funding Council for England. The SDSS web site is http://www.sdss.org/.

REFERENCES

Abazajian K. N. et al., 2009, ApJS, 182, 543
Andrews H. et al., 2013, ApJ, 774, 40
Antonucci R., 1993, ARA&A, 31, 473
Appenzeller I. et al., 1998, The Messenger, 94, 1
Bahcall J. N., Spitzer L., Jr, 1969, ApJ, 156, L63
Bahcall J. N., Kirhakos S., Saxe D. H., Schneider D. P., 1997, ApJ, 479, 642
Barton E. J., Cooke J., 2009, AJ, 138, 1817
Bechtold J., Ellingson E., 1992, ApJ, 396, 20
Bennert N., Canalizo G., Jungwiert B., Stockton A., Schweizer F., Peng C. Y., Lacy M., 2008, ApJ, 677, 846
Bennert V. N., Auger M. W., Treu T., Woo J.-H., Malkan M. A., 2011, ApJ, 742, 107
Bergeron J., Boissé P., 1991, A&A, 243, 344
Bergeron J., Stasińska G., 1986, A&A, 169, 1
Birnboim Y., Dekel A., 2003, MNRAS, 345, 349
Boksenberg A., Sargent W. L. W., 1978, ApJ, 220, 42
Bonning E. W., Shields G. A., Salviander S., 2007, ApJ, 666, L13
Bordoloi R. et al., 2011, ApJ, 743, 10
Bordoloi R., Lilly S. J., Kacprzak G. G., Churchill C. W., 2012, preprint (arXiv:1211.3774)
Bouché N., Murphy M. T., Péroux C., Csabai I., Wild V., 2006, MNRAS, 371, 495
Bowen D. V., Chelouche D., 2011, ApJ, 727, 47
Bowen D. V. et al., 2006, ApJ, 645, L105
Cameron E., 2011, PASA, 28, 128
Canalizo G., Stockton A., 2001, ApJ, 555, 719
Canalizo G., Stockton A., 2013, ApJ, 772, 132
Cardelli J. A., Clayton G. C., Mathis J. S., 1989, ApJ, 345, 245
Cepa J. et al., 2000, Proc. SPIE, 4008, 623
Cepa J. et al., 2003, Proc. SPIE, 4841, 1739
Charlton J. C., Churchill C. W., 1998, ApJ, 499, 181
Charlton J. C., Ding J., Zonak S. G., Churchill C. W., Bond N. A., Rigby J. R., 2003, ApJ, 589, 111
Chelouche D., Ménard B., Bowen D. V., Gnat O., 2008, ApJ, 683, 55
Chen H.-W., 2012, MNRAS, 427, 1238
Chen H.-W., Tinker J. L., 2008, ApJ, 687, 745
Chen H.-W., Helsby J. E., Gauthier J.-R., Shectman S. A., Thompson I. B., Tinker J. L., 2010a, ApJ, 714, 1521
Chen H.-W., Wild V., Tinker J. L., Gauthier J.-R., Helsby J. E., Shectman S. A., Thompson I. B., 2010b, ApJ, 724, L176
Churchill C. W., Vogt S. S., 2001, AJ, 122, 679
Churchill C. W., Mellon R. R., Charlton J. C., Jannuzi B. T., Kirhakos S., Steidel C. C., Schneider D. P., 2000, ApJS, 130, 91
Churchill C. W., Vogt S. S., Charlton J. C., 2003, AJ, 125, 98
Churchill C. W., Kacprzak G. G., Steidel C. C., 2005, in Williams P. R., Shu C.-G., Menard B., eds, Proc. IAU Colloq. 199: Probing Galaxies through Quasar Absorption Lines. Cambridge Univ. Press, Cambridge, p. 24
Churchill C. W., Nielsen N. M., Kacprzak G. G., Trujillo-Gomez S., 2013a, ApJ, 763, L42
Churchill C. W., Trujillo-Gomez S., Nielsen N. M., Kacprzak G. G., 2013b, ApJ, 779, 87
Crenshaw D. M., Kraemer S. B., George I. M., 2003, ARA&A, 41, 117
Crotts A. P. S., 1989, ApJ, 336, 550
De Rosa G., Decarli R., Walter F., Fan X., Jiang L., Kurk J., Pasquali A., Rix H. W., 2011, ApJ, 739, 56
Decarli R., Labita M., Treves A., Falomo R., 2008, MNRAS, 387, 1237
Decarli R., Treves A., Falomo R., 2009, MNRAS, 396, L31
Decarli R., Falomo R., Treves A., Kotilainen J. K., Labita M., Scarpa R., 2010a, MNRAS, 402, 2441
Decarli R., Falomo R., Treves A., Labita M., Kotilainen J. K., Scarpa R., 2010b, MNRAS, 402, 2453
Decarli R., Falomo R., Kotilainen J. K., Hyvönen T., Uslenghi M., Treves A., 2012, Adv. Astron., 2012, 782528
Di Matteo T., Springel V., Hernquist L., 2005, Nature, 433, 604
Dobrzycki A., Bechtold J., 1991, ApJ, 377, L69
Ellison S. L., Ibata R., Pettini M., Lewis G. F., Aracil B., Petitjean P., Srianand R., 2004, A&A, 414, 79
Elvis M., 2000, ApJ, 545, 63
Faber S. M. et al., 2007, ApJ, 665, 265
Falomo R., Kotilainen J., Treves A., 2001, ApJ, 547, 124
Falomo R., Kotilainen J. K., Pagani C., Scarpa R., Treves A., 2004, ApJ, 604, 495
Falomo R., Treves A., Kotilainen J. K., Scarpa R., Uslenghi M., 2008, ApJ, 673, 694
Falomo R., Bettoni D., Karhunen K., Kotilainen J. K., Uslenghi M., 2014, MNRAS, 440, 476
Farina E. P., Falomo R., Decarli R., Treves A., Kotilainen J. K., 2013, MNRAS, 429, 1267
Fasano G., Franceschini A., 1987, MNRAS, 225, 155
Floyd D. J. E., Kukula M. J., Dunlop J. S., McLure R. J., Miller L., Percival W. J., Baum S. A., O'Dea C. P., 2004, MNRAS, 355, 196
Floyd D. J. E., Dunlop J. S., Kukula M. J., Brown M. J. I., McLure R. J., Baum S. A., O'Dea C. P., 2013, MNRAS, 429, 2
Fumagalli M., O'Meara J. M., Prochaska J. X., Worseck G., 2013, ApJ, 775, 78
Gauthier J.-R., 2013, MNRAS, 432, 1444
Gauthier J.-R., Chen H.-W., 2011, MNRAS, 418, 2730
Gauthier J.-R., Chen H.-W., Tinker J. L., 2010, ApJ, 716, 1263

Gehrels N., 1986, ApJ, 303, 336
Häring N., Rix H.-W., 2004, ApJ, 604, L89
Hennawi J. F., Prochaska J. X., 2007, ApJ, 655, 735
Hennawi J. F., Prochaska J. X., 2013, ApJ, 766, 58
Hennawi J. F. et al., 2006a, AJ, 131, 1
Hennawi J. F. et al., 2006b, ApJ, 651, 61
Hernquist L., 1989, Nature, 340, 687
Hutchings J. B., Scholz P., Bianchi L., 2009, AJ, 137, 3533
Hyvönen T., Kotilainen J. K., Örndahl E., Falomo R., Uslenghi M., 2007, A&A, 462, 525
Isobe T., Feigelson E. D., Nelson P. I., 1986, ApJ, 306, 490
Jahnke K., Wisotzki L., 2003, MNRAS, 346, 304
Kacprzak G. G., Churchill C. W., Steidel C. C., Murphy M. T., Evans J. L., 2007, ApJ, 662, 909
Kacprzak G. G., Churchill C. W., Steidel C. C., Murphy M. T., 2008, AJ, 135, 922
Kacprzak G. G., Murphy M. T., Churchill C. W., 2010, MNRAS, 406, 445
Kacprzak G. G., Churchill C. W., Evans J. L., Murphy M. T., Steidel C. C., 2011, MNRAS, 416, 3118
Kacprzak G. G., Churchill C. W., Nielsen N. M., 2012, ApJ, 760, L7
Kaspi S., Smith P. S., Netzer H., Maoz D., Jannuzi B. T., Giveon U., 2000, ApJ, 533, 631
Kauffmann G., Haehnelt M., 2000, MNRAS, 311, 576
Kereš D., Katz N., Weinberg D. H., Davé R., 2005, MNRAS, 363, 2
Kereš D., Katz N., Fardal M., Davé R., Weinberg D. H., 2009, MNRAS, 395, 160
Kotilainen J. K., Falomo R., Labita M., Treves A., Uslenghi M., 2007, ApJ, 660, 1039
Kotilainen J. K., Falomo R., Decarli R., Treves A., Uslenghi M., Scarpa R., 2009, ApJ, 703, 1663
Kotilainen J., Falomo R., Bettoni D., Karhunen K., Uslenghi M., 2013, preprint (arXiv:1302.1366)
Kukula M. J., Dunlop J. S., McLure R. J., Miller L., Percival W. J., Baum S. A., O'Dea C. P., 2001, MNRAS, 326, 1533
Lanzetta K. M., Bowen D., 1990, ApJ, 357, 321
Liske J., Williger G. M., 2001, MNRAS, 328, 653
Lopez S. et al., 2008, ApJ, 679, 1144
Lovegrove E., Simcoe R. A., 2011, ApJ, 740, 3
Lundgren B. F. et al., 2012, ApJ, 760, 49
McLure R. J., Jarvis M. J., 2002, MNRAS, 337, 109
McLure R. J., Kukula M. J., Dunlop J. S., Baum S. A., O'Dea C. P., Hughes D. H., 1999, MNRAS, 308, 377
Mannucci F., Basile F., Poggianti B. M., Cimatti A., Daddi E., Pozzetti L., Vanzi L., 2001, MNRAS, 326, 745
Marconi A., Hunt L. K., 2003, ApJ, 589, L21
Ménard B., Chelouche D., 2009, MNRAS, 393, 808
Ménard B., Wild V., Nestor D., Quider A., Zibetti S., Rao S., Turnshek D., 2011, MNRAS, 417, 801
Monet D. G. et al., 2003, AJ, 125, 984
More S., van den Bosch F. C., Cacciato M., Skibba R., Mo H. J., Yang X., 2011, MNRAS, 410, 210
Moster B. P., Somerville R. S., Maulbetsch C., van den Bosch F. C., Macciò A. V., Naab T., Oser L., 2010, ApJ, 710, 903
Nelson D., Vogelsberger M., Genel S., Sijacki D., Kereš D., Springel V., Hernquist L., 2013, MNRAS, 429, 3353
Nestor D. B., Turnshek D. A., Rao S. M., 2005, ApJ, 628, 637
Nestor D. B., Turnshek D. A., Rao S. M., Quider A. M., 2007, ApJ, 658, 185
Nestor D., Hamann F., Rodriguez Hidalgo P., 2008, MNRAS, 386, 2055
Nestor D. B., Johnson B. D., Wild V., Ménard B., Turnshek D. A., Rao S., Pettini M., 2011, MNRAS, 412, 1559
Nielsen N. M., Churchill C. W., Kacprzak G. G., Murphy M. T., 2013a, ApJ, 776, 114
Nielsen N. M., Churchill C. W., Kacprzak G. G., 2013b, ApJ, 776, 115
Peng C. Y., Impey C. D., Ho L. C., Barton E. J., Rix H.-W., 2006a, ApJ, 640, 114
Peng C. Y., Impey C. D., Rix H.-W., Kochanek C. S., Keeton C. R., Falco E. E., Lehár J., McLeod B. A., 2006b, ApJ, 649, 616
Peterson B. M., 2010, in Peterson B., Somerville R., Storchi-Bergmann T., eds, Proc. IAU Symp. 267, Co-Evolution of Central Black Holes and Galaxies. Cambridge Univ. Press, Cambridge, p. 151
Petitjean P., Bergeron J., 1990, A&A, 231, 309
Prochaska J. X., Hennawi J. F., 2009, ApJ, 690, 1558
Prochaska J. X., Hennawi J. F., Simcoe R. A., 2013a, ApJ, 762, L19
Prochaska J. X. et al., 2013b, ApJ, 776, 136
Prochter G. E., Prochaska J. X., Burles S. M., 2006, ApJ, 639, 766
Rao S. M., Turnshek D. A., 2000, ApJS, 130, 1
Rao S. M., Turnshek D. A., Nestor D. B., 2006, ApJ, 636, 610
Rauch M., Sargent W. L. W., Barlow T. A., Simcoe R. A., 2002, ApJ, 576, 45
Ribaudo J., Lehner N., Howk J. C., Werk J. K., Tripp T. M., Prochaska J. X., Meiring J. D., Tumlinson J., 2011, ApJ, 743, 20
Richards G. T., Vanden Berk D. E., Reichard T. A., Hall P. B., Schneider D. P., SubbaRao M., Thakar A. R., York D. G., 2002, AJ, 124
Rodríguez Hidalgo P., Wessels K., Charlton J. C., Narayanan A., Mshar A., Cucchiara A., Jones T., 2012, MNRAS, 427, 1801
Rubin K. H. R., Weiner B. J., Koo D. C., Martin C. L., Prochaska J. X., Coil A. L., Newman J. A., 2010, ApJ, 719, 1503
Rubin K. H. R., Prochaska J. X., Koo D. C., Phillips A. C., 2012, ApJ, 747, L26
Runnoe J. C., Brotherton M. S., Shang Z., 2012, MNRAS, 422, 478
Sancisi R., Fraternali F., Oosterloo T., van der Hulst T., 2008, A&AR, 15, 18
Sbarufatti B., Treves A., Falomo R., Heidt J., Kotilainen J., Scarpa R., 2005, AJ, 129, 559
Schechter P., 1976, ApJ, 203, 297
Schirber M., Miralda-Escudé J., McDonald P., 2004, ApJ, 610, 105
Schlegel D. J., Finkbeiner D. P., Davis M., 1998, ApJ, 500, 525
Schneider D. P. et al., 1993, ApJS, 87, 45
Schneider D. P. et al., 2010, AJ, 139, 2360
Serber W., Bahcall N., Ménard B., Richards G., 2006, ApJ, 643, 68
Sharma M., Nath B. B., Chand H., 2013, MNRAS, 431, L93
Shaver P. A., Robertson J. G., 1983, ApJ, 268, L57
Shaver P. A., Robertson J. G., 1985, MNRAS, 212, 15p
Shaver P. A., Boksenberg A., Robertson J. G., 1982, ApJ, 261, L7
Shen Y., 2013, Bull. Astron. Soc. India, 41, 61
Shen Y., Ménard B., 2012, ApJ, 748, 131
Steidel C. C., 1995, in Meylan G., ed., QSO Absorption Lines. Springer-Verlag, Berlin, p. 139
Steidel C. C., Sargent W. L. W., 1992, ApJS, 80, 1
Steidel C. C., Dickinson M., Persson S. E., 1994, ApJ, 437, L75
Steidel C. C., Dickinson M., Meyer D. M., Adelberger K. L., Sembach K. R., 1997, ApJ, 480, 568
Steidel C. C., Erb D. K., Shapley A. E., Pettini M., Reddy N., Bogosavljević M., Rudie G. C., Rakic O., 2010, ApJ, 717, 289
Tody D., 1986, Proc. SPIE, 627, 733
Tremonti C. A., Moustakas J., Diamond-Stanic A. M., 2007, ApJ, 663, L77
Tripp T. M., Bowen D. V., 2005, in Williams P. R., Shu C.-G., Menard B., eds, Proc. IAU Colloq. 199: Probing Galaxies through Quasar Absorption Lines. Cambridge Univ. Press, Cambridge, p. 5
Tytler D., Fan X.-M., 1992, ApJS, 79, 1
Tytler D. et al., 2009, MNRAS, 392, 1539
van de Voort F., Schaye J., 2012, MNRAS, 423, 2991
Vanden Berk D. et al., 2008, ApJ, 679, 239
Vestergaard M., 2003, ApJ, 599, 116
Vestergaard M., Peterson B. M., 2006, ApJ, 641, 689
Vestergaard M., Wilkes B. J., 2001, ApJS, 134, 1
Weiner B. J. et al., 2009, ApJ, 692, 187
Werk J. K., Prochaska J. X., Thom C., Tumlinson J., Tripp T. M., O'Meara J. M., Peeples M. S., 2013, ApJS, 204, 17
Wild V. et al., 2008, MNRAS, 388, 227
Wold M., Lacy M., Lilje P. B., Serjeant S., 2001, MNRAS, 323, 23
Zhang S., Wang T., Wang H., Zhou H., 2013, ApJ, 773, 175
Zheng Z., Zehavi I., Eisenstein D. J., Weinberg D. H., Jing Y. P., 2009, ApJ, 707, 554

Zibetti S., Ménard B., Nestor D. B., Quider A. M., Rao S. M., Turnshek D. A., 2007, ApJ, 658, 161
Zwaan M. A., van der Hulst J. M., Briggs F. H., Verheijen M. A. W., Ryan-Weber E. V., 2005, MNRAS, 364, 1467

APPENDIX A: BLACK HOLE MASSES AND BOLOMETRIC LUMINOSITIES OF QUASARS

To determine the black hole masses ($M_{\rm BH}$) and the bolometric luminosity ($L_{\rm bol}$) of the observed quasars, we fitted their spectra following the procedure presented in Decarli et al. (2010a) and in De Rosa et al. (2011). Namely, the quasar emission was composed with a superposition of: (i) a non-stellar continuum, modelled as a power law; (ii) the contribution from Fe II-blended multiplets (assuming the template of Vestergaard & Wilkes 2001); (iii) the stellar light from the host galaxy (assuming the elliptical template of Mannucci et al. 2001); (iv) the broad lines emission (fitted with two Gaussian curves with the same peak wavelength; see Decarli et al. 2008). The results of the fitting procedure allowed us to estimate the $L_{\rm bol}$ from the monochromatic luminosity at 3000 Å (assuming the bolometric correction presented in Runnoe, Brotherton & Shang 2012, see Table 1) and the $M_{\rm BH}$ applying the virial theorem to the gas of the broad-line region (e.g. Kaspi et al. 2000; McLure & Jarvis 2002; Vestergaard & Peterson 2006; Peterson 2010; Shen 2013, and references therein, see Table 1).

APPENDIX B: NOTES ON INDIVIDUAL OBJECTS

In this appendix, we present all the absorption lines detected in the quasar spectra over a 3σ threshold. The properties of the observed systems are listed Table B1.

QQ01 – Several intervening metal absorption lines are present in the $\rm QSO_B$ spectra. The most prominent are an Mg II and two C IV doublets at $z \sim 0.734$, 2.173, and 2.383, and an Fe II multiplet at $z \sim 1.174$.

QQ02 – In the spectra of QQ02F, we detected an Mg II absorption doublet at $z \sim 1.264$. A further one is present at $z \sim 1.602$, $\sim$2000 km s^{-1} bluewards of the Mg II broad emission line. Even if this system does not match the considered velocity constraint (see Section 4), it could be associated with an outflow of gas originated from the quasar itself or from its host galaxy (e.g. Crenshaw, Kraemer & George 2003; Tremonti, Moustakas & Diamond-Stanic 2007; Wild et al. 2008; Shen & Ménard 2012; Sharma, Nath & Chand 2013).

In the spectra of QQ02B, we observe the presence a C IV absorption system ($W_{\rm r}(\lambda1548) = (0.39 \pm 0.09)$ Å) blueshifted by $\sim$700 km s^{-1} with respect to the quasar emission frame. These kinds of features are often detected close the C IV broad emission lines and are thought to arise in quasar outflows (e.g. Vestergaard 2003; Nestor, Hamann & Rodriguez Hidalgo 2008). The identification of the Mg II transverse absorption features associated with $\rm QSO_F$ is sustained by the presence of the Fe II(λ2382) and Fe II(λ2600) lines at the same redshift.

QQ04 – In the spectra of QQ04F, we detect Fe II and Mg II lines produced by an intervening absorption system at $z \sim 1.211$. The identification of the Mg II transverse absorption system is supported

Table B1. Properties of absorption features detected in QSOs spectra over a 3σ level: our identification label of the quasar (ID), observed wavelength ($\lambda_{\rm abs}$), observed equivalent width (W), absorption line (line), and redshift ($z_{\rm abs}$).

ID	$\lambda_{\rm abs}$ (Å)	W (Å)	Line	$z_{\rm abs}$
QQ01B	4850.8	1.01 ± 0.34	Mg II λ2796	0.7349 ± 0.0004
QQ01B	4861.1	1.00 ± 0.34	Mg II λ2803	0.7342 ± 0.0004
QQ01B	4910.4	1.22 ± 0.34	C IV λ1548	2.1721 ± 0.0006
QQ01B	4918.1	1.07 ± 0.35	C IV λ1550	2.1730 ± 0.0006
QQ01B	5096.3	0.61 ± 0.25	Fe II λ2344	1.1742 ± 0.0004
QQ01B	5180.3	0.72 ± 0.29	Fe II λ2382	1.1748 ± 0.0004
QQ01B	5235.4	1.02 ± 0.35	C IV λ1548	2.3820 ± 0.0006
QQ01B	5244.2	1.01 ± 0.35	C IV λ1550	2.3834 ± 0.0006
QQ01B	5444.6	0.70 ± 0.18	–	–
QQ01B	5652.3	0.82 ± 0.26	Fe II λ2600	1.1740 ± 0.0004
QQ01B	5869.9	0.82 ± 0.23	Mg II λ2796	1.0994 ± 0.0005
QQ01B	5881.0	0.52 ± 0.38	Mg II λ2803	1.0981 ± 0.0005
QQ02F	6330.8	0.84 ± 0.20	Mg II λ2796	1.2642 ± 0.0004
QQ02F	6330.8	0.80 ± 0.23	Mg II λ2803	1.2644 ± 0.0004
QQ02F	7275.6	1.34 ± 0.42	Mg II λ2796	1.6021 ± 0.0005
QQ02F	7291.8	0.85 ± 0.42	Mg II λ2803	1.6014 ± 0.0005
QQ02B	5785.9	1.45 ± 0.35	C IV λ1548	2.7377 ± 0.0010
QQ02B	5795.7	1.18 ± 0.32	C IV λ1550	2.7392 ± 0.0009
QQ02B	6086.7	1.03 ± 0.34	–	–
QQ02B	6245.1	0.97 ± 0.31	Fe II λ2382	1.6218 ± 0.0003
QQ02B	6814.9	0.95 ± 0.36	Fe II λ2600	1.6211 ± 0.0003
QQ04F	5718.7	0.76 ± 0.28	Fe II λ2586	1.2114 ± 0.0004
QQ04F	5748.2	1.12 ± 0.32	Fe II λ2600	1.2108 ± 0.0003
QQ04F	6181.9	2.93 ± 0.22	Mg II λ2796	1.2110 ± 0.0002
QQ04F	6198.0	2.36 ± 0.19	Mg II λ2803	1.2112 ± 0.0002
QQ04B	5999.6	0.27 ± 0.13	Fe II λ2586	1.3200 ± 0.0004
QQ04B	6031.0	0.63 ± 0.12	Fe II λ2600	1.3196 ± 0.0004
QQ05B	4878.1	1.61 ± 0.56	Fe II λ2344	1.0811 ± 0.0005
QQ05B	5383.0	0.83 ± 0.32	Fe II λ2586	1.0816 ± 0.0005
QQ05B	5410.7	1.42 ± 0.30	Fe II λ2600	1.0810 ± 0.0003
QQ05B	5818.3	2.60 ± 0.43	Mg II λ2796	1.0809 ± 0.0002
QQ05B	5833.4	2.30 ± 0.32	Mg II λ2803	1.0811 ± 0.0002
QQ07B	4641.8	3.15 ± 0.43	Mg II λ2796?	0.6602 ± 0.0006
QQ07B	4650.7	2.15 ± 0.46	Mg II λ2803?	0.6592 ± 0.0006
QQ07B	4973.9	1.02 ± 0.39	C IV λ1548	2.2131 ± 0.0006
QQ07B	4981.6	0.70 ± 0.18	C IV λ1550	2.2139 ± 0.0006
QQ09B	5287.3	1.61 ± 0.38	Mg II λ2796?	0.8910 ± 0.0005
QQ09B	5296.4	1.35 ± 0.29	C IV λ1548?	2.4214 ± 0.0005
QQ09B	5300.3	0.68 ± 0.22	Mg II λ2803?	0.8909 ± 0.0006
QQ09B	5304.4	1.70 ± 0.38	C IV λ1550?	2.4222 ± 0.0005
QQ09B	5379.6	1.57 ± 0.20	–	–
QQ09B	5389.4	0.92 ± 0.30	Fe II λ2586?	1.0841 ± 0.0003
QQ09B	5419.5	3.39 ± 0.28	Fe II λ2600?	1.0844 ± 0.0003
QQ09B	5642.2	0.99 ± 0.28	–	–
QQ09B	5660.4	2.97 ± 0.38	Si IV λ1393?	3.0622 ± 0.0007
QQ09B	5696.3	1.94 ± 0.37	Si IV λ1402?	3.0622 ± 0.0007
QQ09B	5805.1	2.14 ± 0.37	–	–
QQ10F	4486.2	0.48 ± 0.16	Mg II λ2796	0.6045 ± 0.0003
QQ10F	4497.4	0.50 ± 0.17	Mg II λ2803	0.6045 ± 0.0003
QQ12F	7317.0	2.15 ± 0.56	–	–
QQ12B	6044.5	0.92 ± 0.31	Mg II λ2796?	1.1618 ± 0.0005
QQ12B	6057.4	0.94 ± 0.34	Mg II λ2803?	1.1610 ± 0.0005
QQ14F	5890.3	0.38 ± 0.12	–	–
QQ14B	6983.3	0.77 ± 0.24	Fe II λ2374	1.9416 ± 0.0003
QQ14B	7007.2	1.46 ± 0.22	Fe II λ2382	1.9417 ± 0.0003
QQ16B	5922.1	3.37 ± 0.51	Mg II λ2796	1.1181 ± 0.0003
QQ16B	5938.0	2.75 ± 0.53	Mg II λ2803	1.1184 ± 0.0003
QQ17B	4493.1	1.45 ± 0.49	Fe II λ2586	0.7375 ± 0.0005
QQ17B	4517.9	2.53 ± 0.99	Fe II λ2600	0.7377 ± 0.0007
QQ17B	4858.1	2.22 ± 0.61	Mg II λ2796	0.7375 ± 0.0004

Table B1 – *continued*

ID	λ_{abs} (Å)	W (Å)	Line	z_{abs}
QQ17B	4870.6	1.88 ± 0.81	Mg II λ2803	0.7376 ± 0.0004
QQ17B	5566.4	2.62 ± 0.44	Fe II λ2344	1.3748 ± 0.0004
QQ17B	5637.6	1.22 ± 0.29	Fe II λ2374	1.3747 ± 0.0004
QQ17B	5657.7	3.19 ± 0.46	Fe II λ2382	1.3752 ± 0.0004
QQ18B	6210.9	1.67 ± 0.16	Fe II λ2344	1.6497 ± 0.0004
QQ18B	6291.1	1.10 ± 0.26	Fe II λ2374	1.6500 ± 0.0004
QQ18B	6313.1	2.09 ± 0.29	Fe II λ2382	1.6503 ± 0.0004
QQ18B	6853.3	1.58 ± 0.48	Fe II λ2586	1.6502 ± 0.0004
QQ18B	6888.7	2.86 ± 0.46	Fe II λ2600	1.6495 ± 0.0004
QQ18B	7408.4	2.60 ± 0.19	Mg II λ2796	1.6496 ± 0.0004
QQ18B	7427.6	2.67 ± 0.13	Mg II λ2803	1.6499 ± 0.0004
QQ18B	7558.5	0.75 ± 0.44	Mg I λ2853	1.6493 ± 0.0004

by the detection of the associated Fe II(λ2586) and Fe II(λ2600) lines.

QQ05 – An Mg II and Fe II absorption system is present in the spectra of QQ04B at $z \sim 1.081$.

QQ07 – Two close absorption lines ($\lambda\lambda = 4641.8, 4650.7$Å) are present in the spectra if QQ07B. We tentatively identify these features with an Mg II doublet at $z \sim 0.660$. We also observe a C IV doublet at almost the same redshift of the C IV broad emission line ($z \sim 2.213$). The velocity difference between the quasar frame and the absorber ($\lesssim 200\,km\,s^{-1}$) suggests that we are probing cool gas clouds strictly connected to the quasar itself.

QQ08 – The detection of the [Ne V] forbidden emission line allows us to refine the redshift of the QSO_F: $z = 0.6853 \pm 0.0008$. The redshift of the detected transverse absorption system is consistent, within the uncertainties, with this value.

QQ09 – QQ09B is the highest redshift quasar that we have observed. Its spectra is polluted by the Lyα forest hence recognize the detected absorption lines is challenging. We tentatively identify Mg II, C IV, Fe II, and Si IV doublets at $z \sim 0.891$, 2.421, 1.084, and 3.062, respectively. In particular, the Si IV(λ1402) line is superimposed to the Mg II(λ2796) transverse absorption associated with the QSO_F (see Fig. 3). We decouple the two contribution by fitting the blended lines with two Gaussian at the same time, and matching the width of the Mg II(λ2796) line to that of the Mg II(λ2803) one.

QQ10 – In the spectra of QSO_F, we detect an intervening Mg II absorption system at $z = 0.6045 \pm 0.0002$.

QQ12 – An Mg II absorption feature is present at $z = 1.1618 \pm 0.0004$, $\sim 4500\,km\,s^{-1}$ from the transverse system associated with the QSO_F. As for QQ02F, this doublet does not match our constraint on the velocity difference with the quasar frame, but we cannot exclude that it arise in a strong outflow of gas originated from region close to the SMBH or from its host galaxy.

QQ14 – An absorption line superimposed to the Mg II emission is present in the spectra of QQ14F. The absence of another close absorption line over a 2σ threshold suggests that this features is not an Mg II LOS doublet associated with the QSO_F.

The QSO_F redshift derived from the Mg II broad emission line is consistent with the redshift inferred from the [Ne V] narrow line ($z = 1.1057 \pm 0.0008$).

An Fe II doublet is present in the spectra of QQ14B at $z \sim 1.942$.

QQ16 – Data for this pair were already gathered with FORS2 at ESO-VLT (see Farina et al. 2013). The values of the rest-frame equivalent widths quoted in Table 2 are the weighted mean of the two observations. An Mg II doublet is detected at $z \sim 1.118$ in the QQ16B spectra.

QQ17 – Two absorbing systems at redshift $z \sim 0.737$ and $z \sim 1.375$ are identified in the spectra of QQ17B from the detection of Mg II and Fe II absorption lines.

QQ18 – A strong intervening Mg II absorption system ($W_r(\lambda 2796) = 0.98 \pm 0.07$) is present at $z \sim 1.650$, further confirmed by the detection of the corresponding Fe II and Mg I lines.

APPENDIX C: ESTIMATE OF THE GALACTIC ENVIRONMENT

In order to evaluate the contribution of the close galactic environment to the observed absorption systems, we created a set of 10 000 mock projected quasar pairs with impact parameter uniformly distributed between 20 and 200 kpc. For each foreground quasar, we randomly generated a distribution of galaxies that mimic the projected quasar–galaxy cross-correlation function reported by Zhang et al. (2013), who have explored the fields of quasars at $z \sim 1.1$ down to $\sim M^\star + 1$ (where $M^\star$ is the characteristic absolute magnitude of galaxies). This allowed us to calculate that, on average, less then two galaxies associated with a quasar are present within a projected distance of 400 kpc. The contribution of these galaxies to the strength of the Mg II absorption systems depends on their separation from the background quasar, which is indeed the pencil-beam used to investigate the CGM. This distance permitted us to calculate the $W_r(\lambda 2796)$ associated with each mock galaxy considering the W_r versus pd anticorrelation presented by Chen et al. (2010a) as

$$\log W_r(\lambda 2796) = -(1.17 \pm 0.10)\,\log \mathrm{pd} + (1.28 \pm 0.13). \quad \text{(C1)}$$

In order to reproduce the real distribution of absorbers, to the $W_r(\lambda 2796)$ derived from equation (C1) we added a random scatter term of 0.35 dex that take into account the differences between the observed and the estimated Mg II absorber strength (Chen et al. 2010a). We also considered that the covering fraction of absorbing gas decreases with the increase of the distance from a galaxy, almost vanishing at separation larger than 200 kpc (e.g. Barton & Cooke 2009; Chen et al. 2010a; Steidel et al. 2010; Bordoloi et al. 2011; Nielsen et al. 2013a). To simulate this effect, the fraction of absorbers present at a certain galactocentric radius and with a given equivalent width was tuned to reproduce the covering fraction profiles of the galaxies brighter than $M^\star + 1$ present in the sample of Nielsen et al. (2013b, see Fig. C1). Finally, if more than one galaxy intercept the same LOS, we summed on all the $W_r(\lambda 2796)$ of the contribution (Bordoloi et al. 2011).

In this estimate, we have not considered any dependence of the absorber equivalent widths with the galaxy properties. This represent a second-order correction to the W_r versus pd anticorrelation, and has a negligible influence to our results. We also point out that, in principle, the gas associated with faint galaxies could contribute to observed absorption systems. Indeed, galaxies with absolute magnitude between $M^\star + 1$ and $M^\star + 2$ are almost two times more abundant than luminous galaxies[4] (i.e. brighter than $M^\star + 1$). However, these faint galaxies rarely show Mg II absorbers with $W_r(\lambda 2796) \geq 0.1$ Å at impact parameter larger than 60 kpc (e.g. 1 out of 13 galaxies in the sample of Nielsen et al. 2013b). Given the different size of the CGM, the presence of faint galaxies could affect

[4] Estimated considering a Schechter luminosity function (Schechter 1976) with a faint-end slope $\alpha = -1.30$ (Faber et al. 2007).

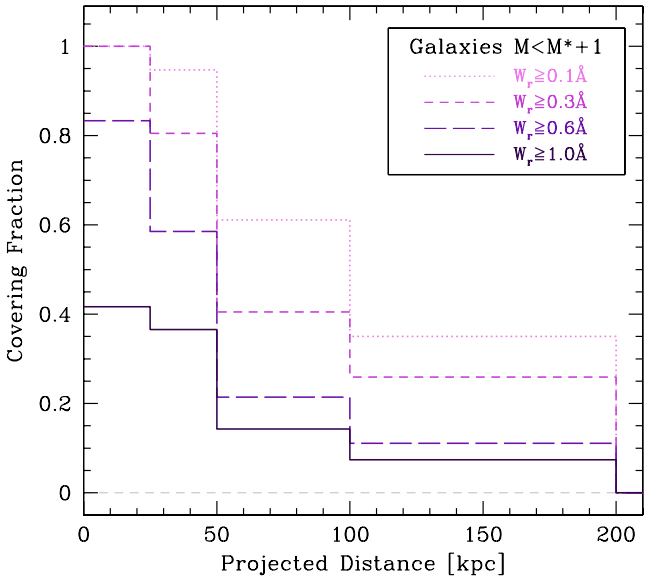

Figure C1. Covering fraction profiles for galaxies brighter than $M^{\star} + 1$ estimated from the sample of Nielsen et al. (2013b). The various shades of violet indicate the different equivalent width limit considered.

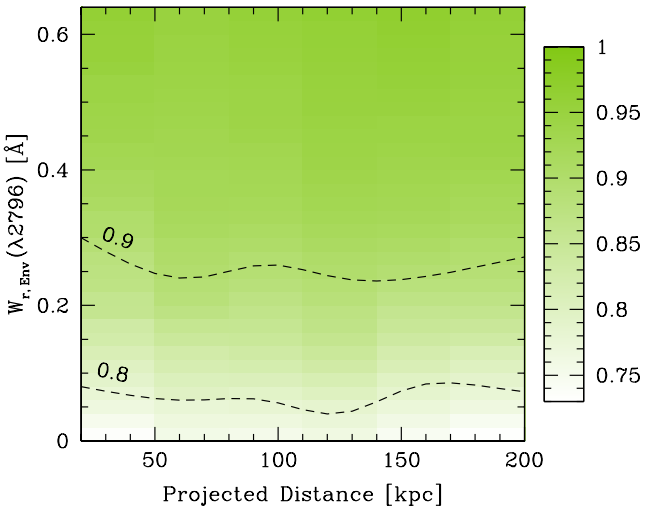

Figure C2. Fraction of simulated galactic environments that contribute to the strength of the transverse absorption systems with an equivalent width $W_{\rm r} \leq W_{\rm r,Env}(\lambda 2796)$ (see Appendix C for details). The cumulative distribution is estimated in bins of 30 kpc each, and the different fractions are colour coded in the bar at the right-hand side of the plot. The two black dashed lines show that the 80 per cent of the systems influence the equivalent width of the detected absorption for less than 0.1 Å and the 90 per cent for less than 0.3 Å.

our estimates for less than ∼15 per cent. In addition, it is worth noting that the sample of isolated galaxies used as comparison in this work derives from different surveys and the magnitude limit of the imaged quasar fields are not uniforms. For instance, ∼40 per cent of the galaxies studied by Nielsen et al. (2013b) come from the sample of Chen et al. (2010a), who used SDSS images to discriminate between isolated and group galaxies, while for ∼30 per cent of the sample deep *Hubble Space Telescope* images are available. This suggests that even some of the galaxies considered as *isolated* could be affected by the contamination of fainter sources.

With these caveats in mind, we estimated that the influence of the environment is of the same order of magnitude of the uncertainties in the $W_{\rm r}(\lambda 2796)$ measurements, and has a negligible influence on our results. Indeed the average contribution of the environment to the associated absorption systems is $W_{\rm r,Env}(\lambda 2796) \lesssim 0.1$ Å, with almost no dependence on the impact parameter. Only ∼25 per cent of the sight lines are covered by absorbing gas associated with satellite galaxies and the covering fractions are $f_{\rm C,Env}(0.30\,\text{Å}) \sim 0.10$ and $f_{\rm C,Env}(0.60\,\text{Å}) \sim 0.05$. As shown in Fig. C2, these values are almost constant in the range of impact parameter explored.

These results confirm that, in average, the influence of the galactic environment is not strong enough to reconcile the differences observed in the CGM of quasars and galaxies. However, deep images of the $\rm QSO_F$ fields are needed to assess the effects of galaxies associated with the quasars on individual absorption systems.

SUPPORTING INFORMATION

Additional Supporting Information may be found in the online version of this article:

Figure 2. Spectra of all the projected quasar pairs corrected for Galactic extinction and binned by 3 pixel. Main quasar emission lines and absorption lines detected over a 3σ threshold are marked (http://mnras.oxfordjournals.org/lookup/suppl/doi:10.1093/mnras/stu585/-/DC1).

Please note: Oxford University Press is not responsible for the content or functionality of any supporting materials supplied by the authors. Any queries (other than missing material) should be directed to the corresponding author for the paper.

This paper has been typeset from a TEX/LATEX file prepared by the author.